Summer 2015

Evaluation of nickel-titanium oxide-niobium pentoxide metal ceramic composite as interconnect for solid oxide fuel cell

Abhijith Budur

Department:

EVALUATION OF NICKEL-TITANIUM OXIDE-NIOBIUM PENTOXIDE METAL CERAMIC COMPOSITE AS INTERCONNECT FOR SOLID OXIDE FUEL CELL

by

ABHIJITH BUDUR

A THESIS

Presented to the Faculty of the Graduate School of the

MISSOURI UNIVERSITY OF SCIENCE AND TECHNOLOGY

In Partial Fulfillment of the Requirements for the Degree

MASTERS

in

MATERIALS SCIENCE AND ENGINEERING

2015

Approved

Dr. Fatih Dogan, Advisor

Dr. F. Scott Miller, Committee member

Dr. Richard K. Brow, Committee member

ABSTRACT

With increasing importance for clean energy, fuel cells have gained great significance in recent decades. Solid oxide fuel cells are easy to transport due to presence of solid electrolyte and also have requisite electrical properties,but have been obstructed by their limitation to be used at only temperatures greater than 600^0C and less than 800^0C. To construct a stack of cells, materials that are good electrical conductors and having necessary mechanical strengths at that temperatures are being considered as interconnects between the cells. Evaluation of Nickel-Titanium dioxide-Niobium pentoxide (NTN) as interconnect and comparison to Stainless Steel 441 alloy has been made in this research. The criteria for evaluation are the resistance, long-term stability and the power density characteristics of the cell for each interconnect. Electrical measurements by impedance spectroscopy techniques were conducted at variousworking temperatures using a gas mixture of 10 % hydrogen and 90% nitrogen to evaluate both interconnect materials in the working range of fuel cells. Scanning Electron Microscopy images of Lanthanum Strontium Manganite paste before and after the fuel cell measurements are shown.The results showed that both NTN and Stainless Steel 441 interconnects exhibit similar electrical properties under operating conditions of the fuel cell. Since theNTN interconnect is less prone to corrosion and does not have the effect of chromium poisoning, it can be considered as a viable interconnect material for solid oxide fuel cells.

ACKNOWLEDGMENTS

I would like to thank my advisor, Dr. Fatih Dogan, for his advice, encouragement and guidance entirely through this study. It was an extreme opportunity for me to work as his research assistant and develop a strong academic background. He created great occasions and support for me to attain technical knowledge which helped me to develop strong foundation on energy materials.

I would like to thank my committee member Dr. Richard K. Brow for adjusting his valuable time in spite of his busy schedule.

I would like to thank my committee member Dr F. Scott Miller for his valuable inputs and helping me in my path.

I owe special thanks to my friends Dheeraj and Pavan for helping me when I needed. I owe great gratitude to Vishnu Priya Talagana for providing me the emotional support and motivation through out my scientific work.

Nothing ends without thanking my family. The final thanks go to my family because of whom, I am here.

Valuable advice, suggestions and support provided by Dr. Nguyen Minh and Dr. Vladimir Petrovsky during the course of this work are much appreciated. This work was supported in part by a grant from the Energy Research & Development Center at Missouri S&T.

TABLE OF CONTENTS

Page

LIST OF ILLUSTRATIONS

LIST OF TABLES

NOMENCLATURE

Symbol	Description
P_x	Partial pressure of 'x'
E	Electro Motive Force (EMF)
z'	Real axis of impedance
z"	Imaginary axis of impedance

1. INTRODUCTION

1.1. BACKGROUND AND OPERATION OF SOLID OXIDE FUEL CELL

Though introduced 150 years ago, major importance to fuel cells has been given in the past two decades. Considering the high potential for portable, green and efficient power generation techniques, fuel cells have attracted great interests as a sustainable energy resource [1,2]. Conversion of chemical energy to electrical energy at high efficiencies, low emissions of sulphuric gases, reduction in emissions of carbon dioxide give fuel cells a significant advantage. Fuel cells that work at high temperature have efficiencies over 60% and superior power densities [3-5].The fuel cells are characterized based upon the material of electrolyte. Solid Oxide Fuel Cell (SOFC) uses a solid oxide electrolyte e.g. ytrria-stabilized zirconia (YSZ). The electrolyte conducts the oxygen ions from cathode to anode. The electrochemical oxidation of these ions with fuel occurs on the anode side.

The fuels used are methane, synthetic gas and hydrogen. Mark et al considered methane, which is a potential fuel for practical applications [6]. The major problems for hydrocarbon fuels are deactivation and loss of cell performance due to deposition of carbon on the anode. Synthetic gas has the same problem of carbon formation. To eliminate this problem, hydrogen can be used as the fuel [7]. The thermodynamic aspects of fuel cell include the temperature and total pressure of fuel (maintained at 1 atmosphere), which affect the voltage of the fuel cell. The thermodynamic aspects of fuel cell will be explained in detail in later sections. Each fuel cell is capable of generating voltage of about 1 V. To get this voltage to working conditions, a stack of fuel cells is to be made. Interconnects are necessary to connect anode of a fuel cell to cathode of the

next fuel cell to build a stack configuration. Figure 1.1 represents the conventional working principle of a fuel cell.

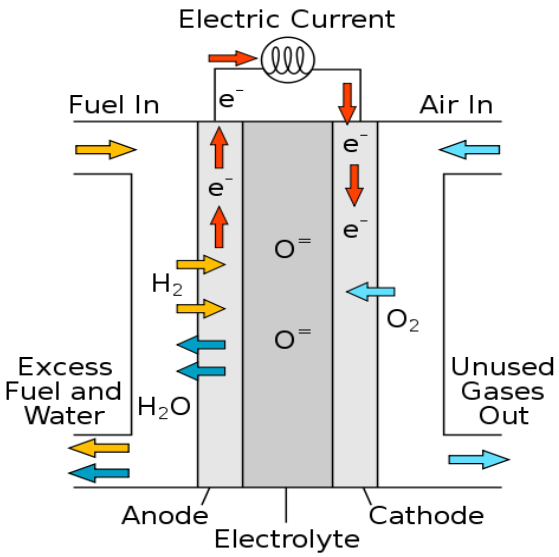

Figure 1. Operation of solid oxide fuel cell

The fuel gets oxidized at the anode of the fuel cell. The oxygen for the oxidation of fuel is obtained from the air at the cathode of fuel cell. The oxygen ions are transported through the electrolyte. The electrons flow through an external circuit from the anode to the cathode, which produces the direct electricity [8]. The three major advantages of SOFCs are: They can use a wide range of fuels i.e. not limited to use of pure hydrogen as fuels. They can be combined as stacks, which provide enough power to use for household applications. The third major advantage is that SOFCs operate at very high temperatures, up to 1000^0C as combined heat and power sources (CHP). The heat given off is also useful for electricity generation in power plants .Any heat added by the SOFC in the

turbine of a power plant replaces heat that would otherwise be supplied by combustion of coal and other fossil fuels.

1.2. THERMODYNAMICS OF SOLID OXIDE FUEL CELL

Under a standard state, the relation between Gibbs free energy change and electromotive force is given with the following reaction

$$\Delta Go = - zFE^o \quad (1)$$

Where E^o is the Electro-Motive Force (EMF) of the standard state, z is the number of electrons transferred and F is Faraday's constant.

Reaction at cathode:

$$\frac{1}{2}O_{2(g)} + 2e' = O^{2-} \quad (2)$$

Reaction at anode:

$$H_{2(g)} + O^{2-} = H_2O + 2e' \quad (3)$$

Overall Reaction:

$$H_{2(g)} + \frac{1}{2}O_{2(g)} = H_2O_{(g)} \quad (4)$$

From this, the Nernst equation for Hydrogen fuel cell is

$$E = E^o - \frac{RT}{2F}\ln\left[\frac{a_{H_2O}}{a_{H_2}.[a_{O_2}]^{\frac{1}{2}}}\right] = E^o - \frac{RT}{2F}\ln\left[\frac{P_{H_2O}}{P_{H_2}.[P_{O_2}]^{\frac{1}{2}}}\right] \quad (5)$$

The equation for voltage is from the thermodynamic data and as a function of temperature and $\frac{P_{H_2O}}{P_{H_2}}$ is

$$E = 1276\text{-}0.32\ T\text{-}0.0429\ T\ \ln\left[\frac{P_{H_2O}}{P_{H_2}}\right](mV) \quad (6)$$

For carbon monoxide fuel cell, the equation for voltage as a function of temperature and $\frac{P_{H_2O}}{P_{H_2}}$ is

$$E = 1460\text{-}0.48\,T\text{-}0.0429T\ln[\frac{P_{CO_2}}{P_{CO}}](mV) \quad (7)$$

Figure 1.2 shows the variations of voltage from oxidation of CO and H_2 with temperature. From the slope of lines in Figure 1.2, the oxidation of carbon monoxide is steeper than the oxidation of hydrogen. Hence it is evident that CO oxidation is more sensitive to temperature than H_2. At 800^0C [standard working temperature for solid oxide fuel cell], both H_2 and CO show similar electrical properties such as fuel cell potential. However H_2 is preferred over CO to eliminate the issue of carbon deposition on the anode [8]. All thermodynamic data for this calculation is taken from reference 9.

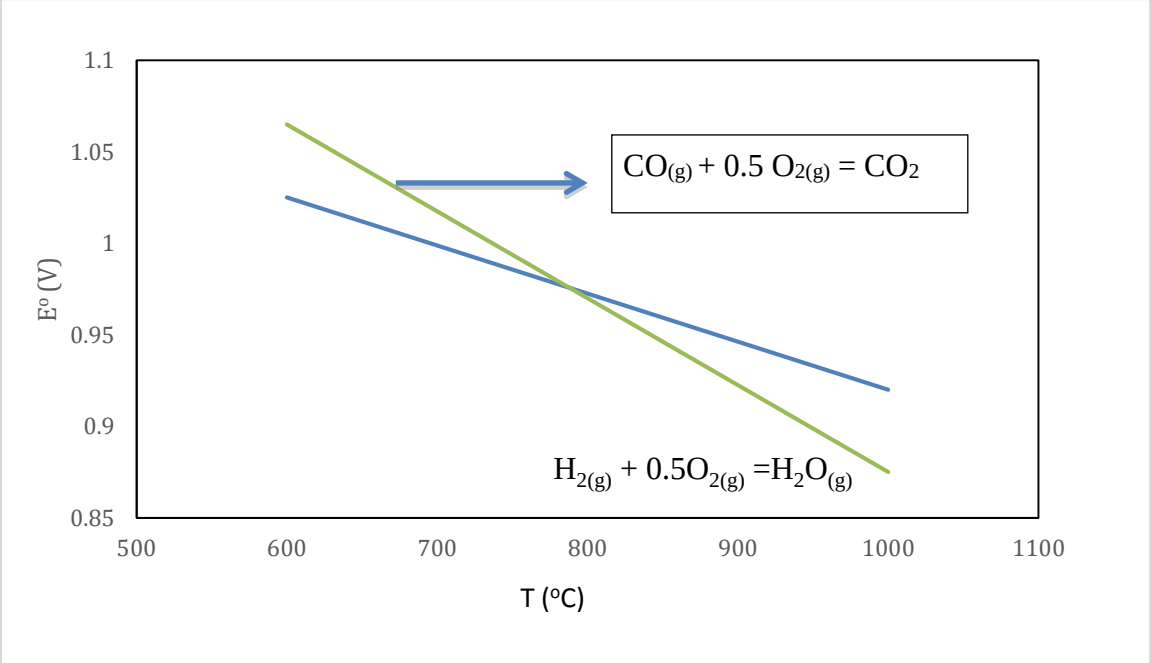

Figure 1.2 Variation of cell potential with temperature and fuels

When the temperature of fuel cell is changed, E values for a specific fuel can be calculated with known parameters. Figure 1.2 illustrates how the voltage of H_2 oxidation process changes with temperature, $\frac{P_{H_2O}}{P_{H_2}}$ respectively, with oxygen partial pressure remaining constant [P_{O_2}=0.21atm, On the cathode side of fuel cell]. E decreases with $\frac{P_{H_2O}}{P_{H_2}}$ in hydrogen fuel cell and temperature. In Figure 1.3 the variation of EMF with temperature and $\frac{P_{H_2O}}{P_{H_2}}$ is exploited.

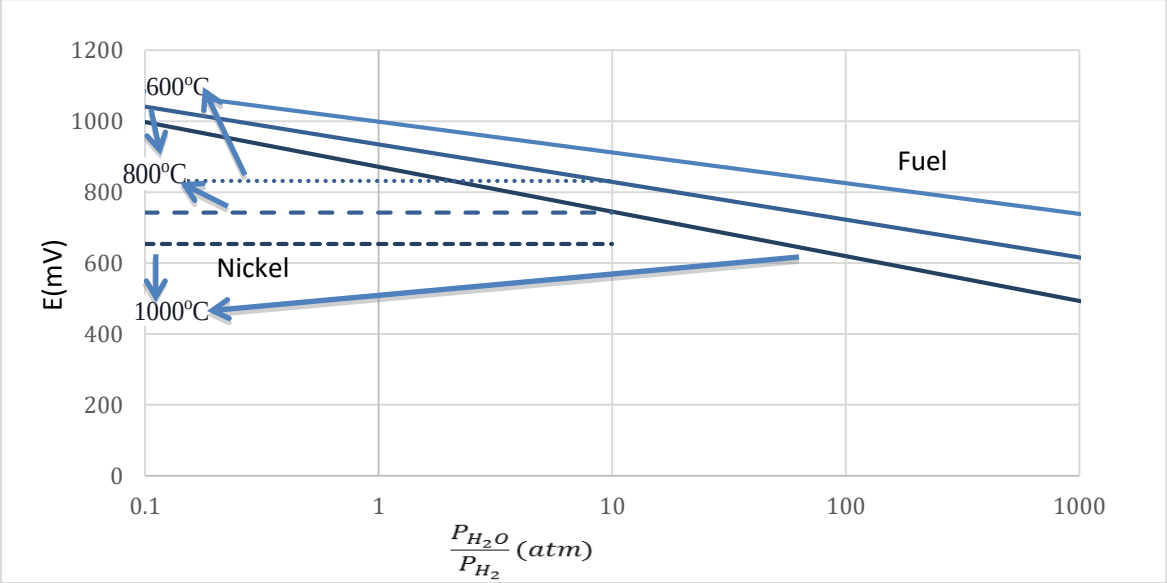

Figure 1.3 Variation of cellpotential with temperature and partial pressure ratio

In a hydrogen fuel cell, the oxidation of $\frac{P_{H_2O}}{P_{H_2}}$must be below the range where the oxidation of nickel-based anode occurs. In the figure 1.3, E_{Ni} (EMF for Nickel oxidation in air shown in dotted lines.) is also plotted. Below the point of Ni-NiO equilibrium the oxidation of Nickel takes place and above it the oxidation of fuel takes place. For

example, a mixture of 99% water vapor and 1% Hydrogen [$\frac{P_{H_2O}}{P_{H_2}}$ = 99 approx] will result in oxidation of Ni metal at 1000^0C. From the Gibbs phase rule, there is only one independent variable in this case [isobaric condition, Ni and NiO are solids]. Hence, E_{Ni} value for a fixed oxygen partial pressures [P_{O_2}=0.21 atm] is dependent only ontemperature and independent of $\frac{P_{H_2O}}{P_{H_2}}$. Once the oxidation of Nickel occurs, the voltage of a cell becomes invariant.

1.3. ELECTROCHEMICAL IMPEDANCE SPECTROSCOPY

To analyze the electrical properties of interconnects, Electrochemical Impedance Spectroscopy (EIS) is used. There are multiple sources of voltage losses in fuel cell. EIS is an experimental technique that provides information on the polarization resistance of the cells. The advantages of this method include: (i) the ability to make high precision measurements because the response may not be perfectly steady and can therefore be averaged over a long term, (ii) the ability to treat the response theoretically by linearizing current-potential characteristics, (iii) measurements can be taken over a wide frequency range.

The EIS method takes advantage of the fact that the polarization loss mechanisms taking place in an electrochemical system differ in their characteristic time constant and frequency response. This measurement is generally performed for a discrete quantity of frequency values in a defined frequency range and the recorded impedance values are usually plotted in the complex plane. The resulting curve is also known as Nyquist-plot as shown in the Figure 1.4.

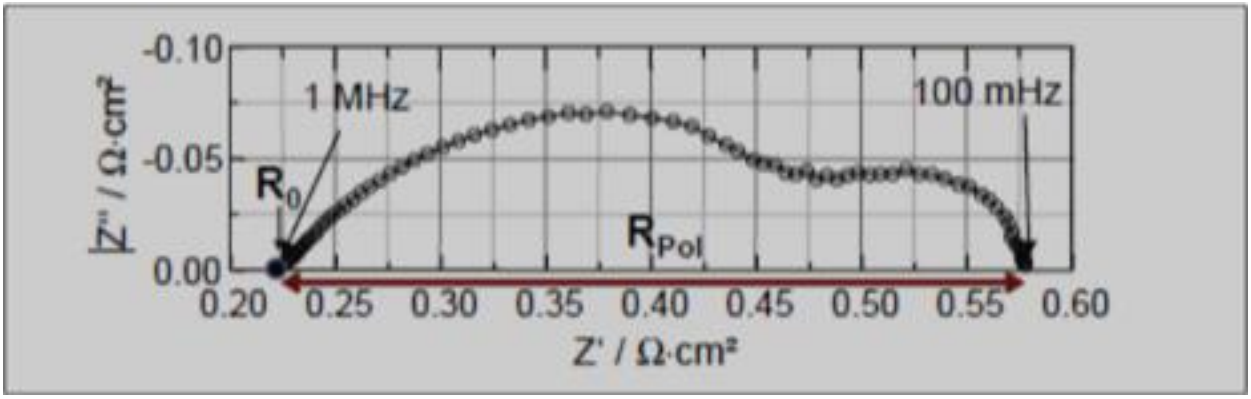

Figure 1.4 Nyquist plot for anode supported solid oxide fuel cell [2]

Fig. 1.4 gives an example Typical Nyquist-plot recorded on an anode supported SOFC single cell. The high frequency intercept (for $\omega \rightarrow \infty$) with the real axis corresponds to the purely ohmic resistance R_0. The difference between the low and high frequency intercept is the so-called polarization resistance R_{pol} of the cell.

Under an operating condition, ohmic, anode and cathode resistances of SOFC can be determined using EIS. The potentiostat applies a galvanic DC current in the same direction as in the SOFC operation during frequency sweeping. Since the processing times for anode and cathode are different, the spectrum generally yields two distinct semi circles. The anode process occurs at a higher frequency range and the cathode process occurs at a lower frequency range, including that the cathode polarization is a slower process.

A typical V-I curve of an SOFC can be measured under a galvanic or a potentiostatic mode. A load bank with a variable resistor gives a constant current to the fuel cell while the voltage is being measured. The voltage pursued is between 0-1V.

1.4. PROPERTIES OF INTERCONNECTS

Fabrication of interconnect is a major challenge considering the high temperatures (800^0C-1000^0C) at which the SOFCs typically operates [10]. Primary function of interconnect is to carry the current in a stack between the fuel cells and also between fuel cell and external circuit. An interconnect needs to be chemically and mechanically stable at the working temperatures for a longer periods of time. This is particularly challenging because interconnect is exposed to oxidizing conditions at cathode and reducing conditions at anode. The thermal expansion of interconnect should match with the thermal expansion coefficient of the other fuel cell materials. A differential expansion will induce mechanical stress and result in a loss of contact area. The thermal expansion coefficient of the interconnect must be close to that of Yttrium Stabilized Zirconia (~ 9 X 10^{-6} K^{-1} at 800^0C) [11] which is used as electrolyte in fuel cells. Apart from thermal expansion the mechanical strength should be good enough to avoid fractures. Though interconnects are not much load bearing components, moderate mechanical strength is required to avoid fractures during stresses by thermal expansion(~9 X $10^{-6}K^{-1}$ to 12 X $10^{-6}K^{-1}$ at 800^0C) [11].

Sealing of the high temperature solid oxide fuel cells stacks is a critical issue to maintain the electrical performance of fuel cell and stability over a long period of time. In fuel cell, the sealant will always be exposed to an oxidizing atmosphere on the cathode side and a fuel gas containing various ratios of hydrocarbons on the anode side. In the cases where hydrogen (10% H_2 and 90% N_2) is used as fuel, the anode will be exposed to a mixture of hydrogen and nitrogen. Some hydrogen must always be maintained in the anode component in order to prevent the oxidation of Ni to NiO. Repeated heating and

cooling of the stack of fuel cells will induce thermal stresses, which can degrade or fracture the sealants. Long time material interactions can also degrade the seals [6].

In this research, interconnect developed by Solid Cell Inc, Rochester, NY has been tested and compared with ferritic steel (SS441). The interconnect material is a ceramic metal composite. The nominal composition as provided by the company is $Ni–TiO_2 – Nb_2O_5$ (NTN). The molar composition of the interconnect is 0.22 Ni, 0.76 TiO_2 and 0.02 Nb_2O_5. The operating temperature is suggested to be less than 950^0C and greater than 650^0C. The density of the interconnect is around 5.43gm/cm^3 and the melting point is around 1455^0C. The contact paste between the interconnect materials and cathode is lanthanum strontium manganite (LSM) that has been studied by scanning electron microscopy (SEM) techniques. The electrical performance of NTN interconnect is compared to a Stainless Steel 441 interconnect.

2. LITERATURE REVIEW

Two types of interconnects are widely used in solid oxide fuel cells. They are ceramic and metallic interconnects [12-14]. Ceramic interconnects are made of semiconducting oxides, which have high resistance towards corrosion and also are compatible with solid oxide fuel cells components in terms of thermal expansion. The primary reason for using the semiconducting oxides as interconnect is that the electrical conductivity of semiconducting oxides increases with increasing temperature suitable for solid oxide fuel cells. But the decrease in conductivity with decreasing temperature puts a limitation on low or intermediate temperature solid oxide fuel cells. The metallic interconnects with potential interests are Nickel, Iron and Chromium based oxidation resistant alloys. Except silver, using the precious metals as an interconnect will not be economical. Though lower cost of silver compared to other materials provides an advantage to use silver, its low melting point and high volatility at the operating temperatures of fuel cell [15,16] and intrinsic instability under hydrogen exposure conditions [17,18] makes silver unacceptable. The major challenge with using metals as interconnect is their resistance to corrosion at high temperatures. Though metals are excellent electrical conductors, corrosion of metals and formation of oxide layers on the surface of interconnects at high temperatures will lower conductivity [19, 20]. Addition of chromium to steels provides good resistance towards oxidation but it has some serious issues regarding the chromium poisoning of the fuel cell. Chromium poisoning is a gas transport phenomenon in which the chromium from the interconnect gets deposited on the cathode. This occurs through the transport of Cr^{+6} containing species in the form of$CrO_{3\,(g)}$, $CrO_2(OH)_{2\,(g)}$. Formation of these volatile species from the oxidation of the

interconnect [21-24] is the main reason for the deposition of chromium on the cathode. The chromium poisoning has been observed in chromium based [25-26], iron based [27] and nickel based alloys [28, 29]. The chromium displacement at the cathode/electrolyte interface is caused by the decrease in oxygen activity at the cathode/electrolyte interface by the cell discharge [30]. In the studies made by Badwal et al. [31] the effect of chromium poisoning was very rapid on the airside if the chromia forming alloys are used as interconnects. It has been suggested that in order to use these alloys, protective coating that are impervious to gases with low diffusion rates for oxygen and chromium should be applied.

Previous research [32] on stainless steels as an interconnect for a fuel cell has shown that specific alloys can be used as interconnect if they are coated with protective coatings. A brief review on most of the protective coatings is given in reference 33. The materials that are used as coating include reactive element oxides [34-38], conductive perovskites [39-48], and conductive spinels [49-57]. Of all these, conductive perovskites are preferred in stainless steels because of the ability to react with chromium and form a conductive layer which helps in reducing chromium poisoning. Lanthanum strontium manganite paste, a conductive perovskite, is used as the coating for interconnects. Apart from protecting the interconnect, the coatings help to reduce the chromium poisoning and also increase the contact area between the interconnect and the cathode.

Though much research on ceramic interconnect materials still needs to be done, ceramic interconnects have a high thermal stability. Ceramics, in general, are inert towards corrosion and other chemical reactions in both oxidizing and reducing atmospheres. Also, the mechanical stability of ceramic interconnects is sufficient to be

used as a fuel cell interconnect. The major drawbacks of using a ceramic interconnect is the low coefficient of thermal expansion. As mentioned, the coefficient of thermal expansion of interconnect is expected to be approximately equal to that of the fuel cell. Since the coefficient of thermal expansion of ceramic materials is low(CTE of $LaCrO_3$~ 5 X 10^{-6} K^{-1} at 800^0C) [11], it cannot be plainly preferred as interconnect for fuel cell. Doping lanthanum with either calcium or strontium increases the CTE, which is desirable since the CTE of YSZ is higher than that of undoped lanthanum chromite. Although there are different significant variations between the CTE reports, the CTE of strontium doped lanthanum chromite is typically larger than that of calcium doped lanthanum chromite, so less strontium is required to increase the CTE to mismatch that of YSZ[57-59]. The ceria additions to calcium doped lanthanum chromite leads to an increase in conductivity and the CTE, so that the dopant level can be optimized to maintain an acceptable level of thermal stress.

The stresses associated with changes in temperatures and oxygen partial pressures cannot be completely eliminated, so the mechanical properties of the interconnect are important for durability. Comparison of the high temperature strength of lanthanum chromite with various dopants shows that the highest strength is obtained by doping with magnesium, followed by strontium [59]. Strontium doped lanthanum chromite also maintains strength at low oxygen partial pressures better than calcium-doped lanthanum chromite.

Pure $LaCrO_3$ is stable to oxygen partial pressures as low as 10^{-21} atmospheres at 1000^0C and thus it is stable in fuel cell environments [62]. The solubility of dopant ions, which are added to increase the conductivity, decrease with increasing oxygen partial

pressure. Of the two most common dopants, calcium and strontium, strontium has the higher solubility at high-oxygen partial pressures, whereas calcium has the higher solubility at low-oxygen partial pressures [62, 63]. The ceramic interconnect material is in contact with both electrodes at elevated temperatures, so chemical compatibility with other fuel cell components is important. Although direct reaction of lanthanum chromite based materials with other components is typically not a major problem, reaction between calcium doped lanthanum chromite and YSZ has been observed [60-62]. Strontium doping, rather than calcium doping, tends to improve the resistance to the reaction, but reaction can occur with strontium doping, especially if $SrCrO_4$ forms on the interconnect [63].

Apart from that, thermal and electrical conductivities of ceramic interconnects are relatively low. Addition of metal to ceramic to form a ceramic-metal composite provides a feasible solution to fabricate the materials to be used as interconnect. Addition of metals increases the electrical conductivity and the plasticity of the composite. The ceramic materials have high fragility, which limits their use as interconnects. Addition of metals induces ductility to the composite interconnects. The ceramic metal composites would utilize full properties of both metals and ceramics; good thermal stability, significant mechanical strength, adjustable thermal expansion (depending upon the addition of metal to the ceramic), good electrical and thermal conductivity, and high toughness. A ceramic metallic composite interconnect gives the choice of variable coefficient of thermal expansion. Depending upon the ratio of metal to ceramic ratio, the coefficient of the thermal expansion that is equal to that of other fuel cell materials can be attained.

The objectives of this study are to compare the electrical properties (power density, area specific resistance) and long term stability of the electrical properties of the NTN interconnect to SS441 interconnect which is the industry standard.

3. EXPERIMENTAL PROCEDURES

3.1. PREPARATION OF INTERCONNECTS

The Lanthanum Strontium Manganite paste and platinum paste used for this study were brought from Fuel Cell Materials Inc. Ohio. LSM paste has a particle size of 0.3-0.6 microns with the solids content 62-72% by weight. Platinum paste has a particle size of 0.8-1.5 microns. In this study the NTN and SS441 interconnects purchased from Solid Cell Inc, Rochester, NY. were used. The interconnect material is a ceramic metal composite.

The nominal composition as provided by the company is $Ni–TiO_2 –Nb_2O_5$(NTN). The molar composition of the interconnect is 0.22 Ni, 0.76 TiO_2 and 0.02 Nb_2O_5. The operating temperature is suggested to be less than 950^0C and greater than 650^0C. The density of the interconnect is around 5.43gm/cm^3 and the melting point is around 1455^0C. A CTE value of NTN provided by Solid Cell Inc. is 10 X 10^{-6} K^{-1}over the working range of the fuel cell, which is near equal to the CTE required. The comparison standard interconnect that is used to compare electrical properties of NTN is SS441 interconnect which is the industrial standard [19]. The CTE and other mechanical properties of the NTN interconnect are similar to that of the SS441 interconnect. The electrical properties (power density, area specific resistance) and long-term stability of the electrical properties of the ceramic composite were compared to the industry standard SS441. NTN and SS441 interconnect coupons were machined to circular discs of dimensions (7 mm diameter & 1 mm thickness).

After cleaning the surface with alcohol, the dimensions of the sample were measured and recorded. Samples were painted with platinum paste to provide contact and

mechanical support to the wires on one side and placed in a furnace for sintering of platinum paste at temperatures and time as shown in Table3.1. All these interconnects were prepared in the similar method.

After sintering the interconnect samples in air, they were painted with Lanthanum Strontium Manganite contact paste to a thickness of ~1 mm and heated at 150^{o}C for 6 hours.

Table 3.1 Sintering conditions of platinum paste on NTN and SS441 interconnects

Temperature (^{o}C)	**Time to attain temperature (hours)**	**Hold time at temperature(hours)**
150	2	2
300	1.5	2
450	1	2
600	4	12
450	2	3
200	2	1
25	2	-

3.2. PREPARATION OF ANODE SUPPORTED SOLID OXIDE FUEL CELL

The fuel cell considered for this experiment is an anode supported solid oxide fuel cellas shown inFigure 3.1. There are three cathodes (Lanthanum Strontium Manganite) printed on the electrolyte (Yittria Stabilized Zirconia) supported on composite anode (NiO+Yittria Stabilized Zirconia). The fuel cells for this research were supplied by Solid Cell Inc. The thickness of the cathode and electrolyte is around 20μm whileanode isaround 200μm thick and the entire fuel cell is around 0.3mm thick.Each of the cathode

is approximately the same diameter of the interconnect i.e., 7mm. One of the cathodes and anode were painted with platinum paste on the fuel cell to attach Pt-Rh wires. The sample was sintered using the temperature profile shown in Table 3.2. After sintering of platinum paste, Pt-Rh wires of 8 cm lengthand 0.5mm diameter were attached both to the cathode and anode. A second layer of platinum coating was painted on the wires and sintered as described in Table 3.2.

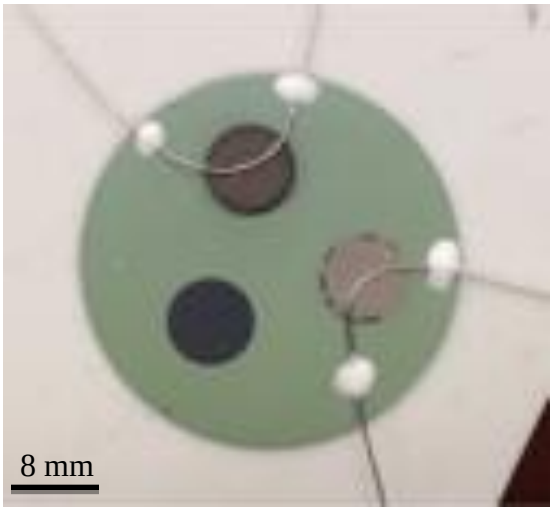

Figure 3.1 Anode supported SOFC and Pt-Rh wires attached to cathode

Table 3.2 Sintering conditions of platinum paste on solid oxide fuel cell

Temperature (°C)	**Time to attain temperature (in hours)**	**Hold time at temperature(hours)**
200	1.5	1.5
400	1.5	1.5
600	1	2
800	3	12
500	2	3
250	2	1
25	2	-

3.3. EXPERIMENTAL SETUP

The NTN and SS441 interconnects were placed on two cathodes. Provisions for four probe current and voltage measurements were done from the cathodes and anode. The fuel cell sample was sealed with a high temperature ceramic cement on to an alumina tube with the diameter same as that of the fuel cell. A specially designed fixture was made for feeding the fuel gas and releasing the exhaust gas to the alumina tube through a complex fitting. Sealing of the ceramic cement was reinforced using a glass bond paint, which fills in the holes formed by the ceramic bond at high temperatures. An alumina plate was used to apply mechanical pressure onto the interconnects. The mechanical load was equal on both interconnects and was achieved using springs. This complete set up was placed in an isothermal zone of a furnace. The furnace was operated using the temperature time profile shown in Table 3.3.The fixture to hold the sample and electrical wiring is shown in Figure 3.2.

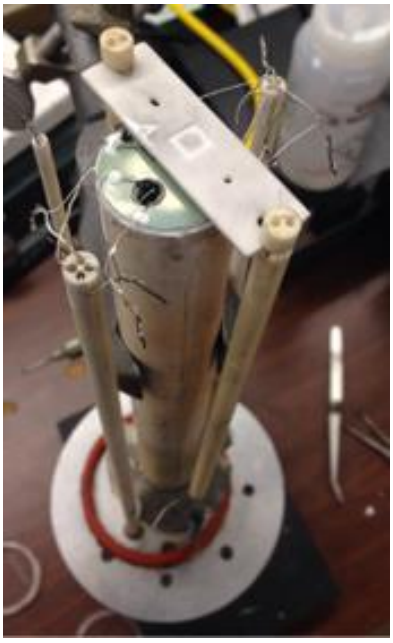

Figure 3.2 Alumina tube mounted with SOFC and fixture to clamp the interconnects

Table 3.3 Temperature - time for the operation

Temperature (°C)	**Time to attain temperature (in hours)**	**Hold time at temperature(hours)**
200	1.5	1.5
500	2	6
600	1	100
675	3	500
725	3	500
800	2	1800

Reduction of the anode, NiO to Ni was achieved through a controlled temperature ramp in an anode flow of 10% Hydrogen and 90% Nitrogen at 500^0C. Controlled reduction of NiO is essential to promote high anode conductivity and sufficient porosity.

After the anode reduction was complete, the cell was brought to the desired temperature for testing. The cathode chamber was not sealed, so stream of air was blown over the surface to ensure ample oxygen availability. Impedance spectroscopy and power density measurements of the cells were conducted using both interconnects and compared with the third cathode with platinum contact paste as a control interconnect.

Each fuel cell tested has three cathodes printed onto it. To avoid experimental errors, most of the comparisons were made between the interconnects on the same fuel cell. This allows a comparison between the interconnects under the same environmental conditions.

Electrochemical testing of the cells was conducted at 800°C using Solartron Analytical 1470 CellTest frequency analyzer. The measurements taken in this case are four probe measurements instead of two probe measurements. The overall impedance measured will be limited to a range of frequency (1 mHz to 1 MHz). Within this frequency range, a frequency sweep is made with logarithmic or linear spacing. This increases the efficiency of measurements for resistances under 1 ohm. A total of four samples were measured for this research.

3.4. SCANNING ELECTRON MICROSCOPY (SEM) AND XRD

The microstructures of the samples were analyzed by SEM techniques and Energy Dispersive Spectroscopy (EDS). The microscope used to take the images is a Helios Nano Lab 600. For each sample, the focus, stigmation, aperture, brightness and contrast were adjusted to capture high clarity images. The first sample was positioned under the beam using the stage controls followed by adjusting the working distance. The image was

focused at specific magnification with the acceleration voltage of 15 kV by correcting for stigmatism. Images of different samples were captured at different magnification levels using the same procedure.

To perform the analysis, after locating the sample at low magnification, a working distance of 4.9 mm was set. Quantitative analysis of the sample was performed with the INCA software. After focusing the image, a necessary magnification spectrum was acquired for the qualitative analysis. The microscope used for taking the images is a Helios NanoLab DualBeam. The conditions of the microscope are defined in the following Table 3.4.

Table 3.4 Working conditions of the electron microscope

Accelerating voltage	5, 10, 15 kV
Working distance	5-7 mm
Mode	Analysis/ Normal
Beam Current	20 μA
Resolution	256 X 200

NTN sample was also characterized by X-ray diffraction (XRD) to identify phases. The diffractometer used to measure for the XRD measurements is the PANalytical X'Pert Diffractometer. The scans were taken from 5^{o} to 90^{o}.

4. RESULTS AND DISCUSSION

4.1. IMPEDANCE SPECTRA

4.1.1. Analysis of Impedance Spectra. Figure 4.1 shows the theoretical impedance spectrum of anode supported SOFC. The graph shows two distinct semi circles, which correspond to the processes in the fuel cell. The ohmic resistance (R_{ohmic}) is the resistance caused by the electrolyte, interconnect and the contact resistances. The electrode process is in general more complicated than the electrolyte counterpart. Each semicircle refers to a single polarization process of either the anode or the cathode. The horizontal axis in the impedance spectrum refers to the resistance and the vertical axis is an imaginary axis that represents the reactance. For an anode supported SOFC, performing of Electrochemical Impedance Spectroscopy (EIS) is simple compared to that of electrolyte supported SOFC. This is because, compared to tubular SOFCs anode supported SOFC have more suitable structure for electrical measurements. Since the surface of the interconnect is planar, fabrication of interconnects will be easier. Within this frequency range, a frequency sweep is made with logarithmic or linear spacing. The impedance data are fitted to a model of equivalent circuit which is normalized to unit area. Of the range of frequency that is swept, the electrode processes dominate the process of electrolyte. The cathode process occurs at lower frequencies and the anode dominates at higher frequencies. This concludes that the cathode polarization is a slower process [2]. The values of resistances can be determined by from analyzing a fitting circuit that is used to fit the impedance spectrum of the fuel cell, which was done using Zview software.

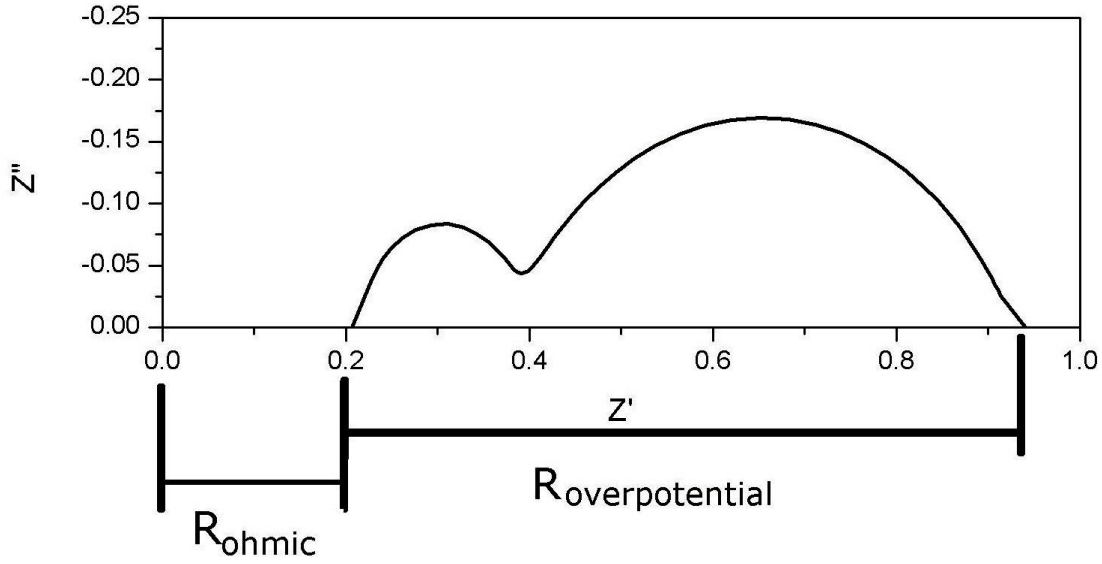

Figure 4.1 Impedance spectrum of anode supported solid oxide fuel cell [3]

The fitting circuit that was used is shown in the Figure 4.2. The initial resistance (R1) corresponds to the combined resistance of electrolyte, interconnect and the contact resistances combined. The resistance-R2 and constant phase element-CPE1 corresponds to the anode process. The resistance-R3 and constant phase elements-CPE 2 corresponds to cathode process. There is not a unique equivalent circuit that describes each spectrum. Therefore it cannot be assumed that an equivalent circuit that produces a good fit to a data set represents an accurate physical model of the cell. But reducing the error percentage can be done by improving the fitting circuit. A fitting model can always be made to look more accurate by adding additional circuit elements to a model. Unfortunately, these elements may have little relevance to the cell processes and it becomes difficult to study the necessary processes. Hence the fitting circuit must be made with the fewest elements possible. In this research most of the importance is given to R1 values since it represents the resistance of the electrolyte and the interconnect.

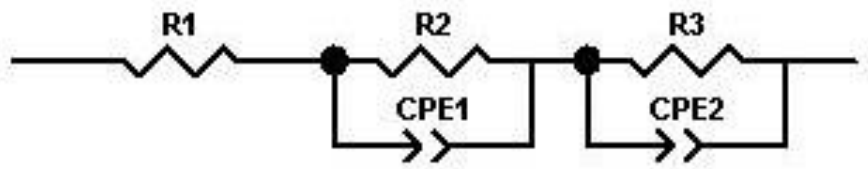

Figure 4.2 Fitting circuit that is used to calculate the resistance values

Figure 4.3 shows the fitting curve of NTN interconnect on the cathode at 800^0C from sample 2. Though two semi circles are not clearly visible, it can be seen that the cathode polarization is a much slower process. The respective resistances have been identified in the figure. The anodic process occurs at higher frequencies as a relatively fast process. The values of the resistances along with the respective errors are depicted in the Table 4.1. The main focus of this research is measurement of the resistance of combined electrolyte and interconnects. The changes in the cathode impedance are due to degradation of the cathode including possible chromium poisoning. Chromium poisoning is avoided by using NTN interconnect because of absence of chromium in the interconnect.

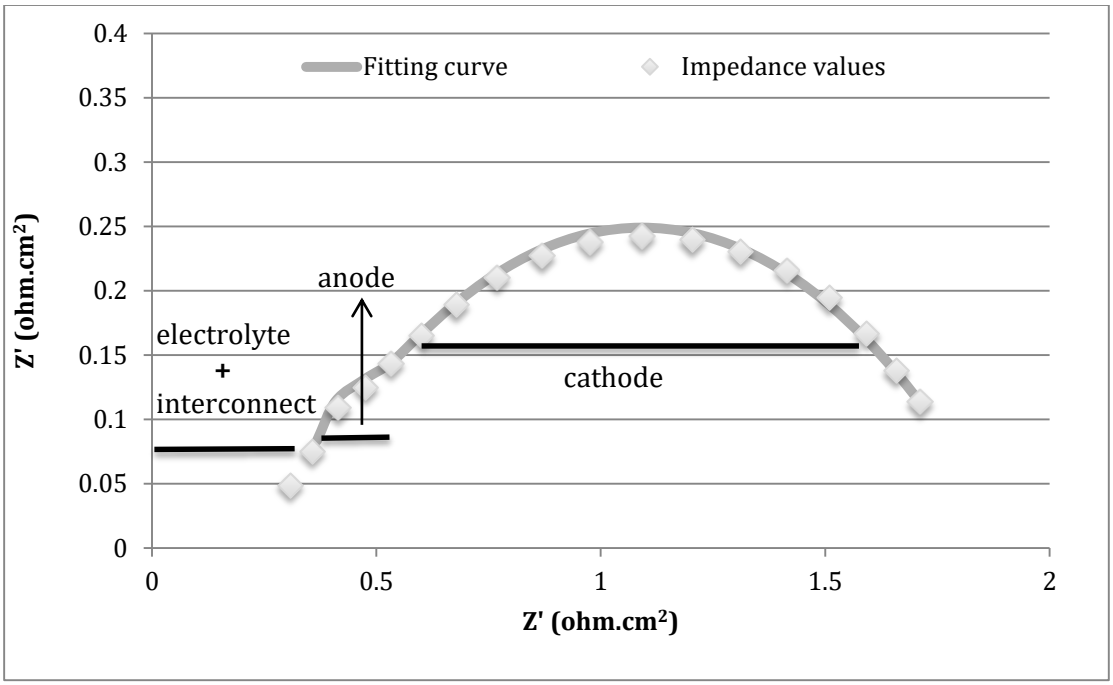

Figure 4.3 Impedance spectrum of NTN interconnect on SOFC at 800^0C

The area specific resistance values in Table 4.1 correspond to a fuel cell with NTN interconnect. The value of error percentage is calculated from the fit between the fitting circuit and the impedance spectrum. A zero percentage error indicates a perfect fit and the values are correct to null error.

Table 4.1 Resistance values determined from the fitting curve

	Area specific resistance (ohm. cm^2)	Error correction
R1 (electrolyte + interconnect)	0.244	±1.53
R2 (anode)	0.131	±2.68
R3 (cathode)	1.221	±5.97

From the values of resistance, it is clear that the sensitivity of data is very high and there is a high probability of experimental errors. Due to the sensitivity of the data, the electrical resistance from the wires should be kept as low as possible. Corrosion on the wires could be a serious cause to increase the electrical resistance. Platinum-Rhodium wires are significantly resistant towards corrosion, which makes them suitable to carry out electrical measurements. Environmental conditions surrounding the fuel cell also affect the value of electrical resistance, which will result in random increase, or decrease of resistance. The approximations of the fitting values vary within an error of 8%. This error is calculated on the total value of the electrolyte, the interconnect and the contact resistances.

4.1.2. Impedance Spectra of Fuel Cell and Interconnects. The electrical performance of the interconnects on the solid oxide fuel cell was evaluated via area specific resistance measurements. The specific impedance values for the NTN, SS441 and the fuel cell are shown in Figures 4.4, 4.5 and 4.6 at three different temperatures. Within each graph there are multiple spectra showing the different temperatures at which the measurements are made. Thus, results from total of nine plots are shown in these graphs. The multiple temperature samples are identified by same shape of markers for each temperature. The measurements of area specific resistances were conducted with a temperature range of 675°C and 800°C.The data were taken after 400 hours of cell operation. The horizontal axis represents the real part of impedance spectrum and the vertical axis represents the imaginary part. The measurements are made with interconnect attached to the cathode of the fuel cell. These values are compared with the impedance values of SS441 interconnect.

Figure 4.4 gives the plots of impedance spectrum of the fuel cell without NTN interconnect. From these spectra the values of resistances are measured with a similar simulated circuit as in Figure 4.2 and the R1 values from the simulated circuit gives the electrolyte and other contact resistances. R2 and R3 resistances give the values of resistances of anode and cathode respectively. Since the process in anode and cathode is a polarization process, the resistance of cathode and anode will not be effected by the presence of the interconnect. R1 value, which encapsulates the resistance of electrolyte and other contact resistances and is affected by the presence of the interconnect. To find out the net effective resistance of the interconnect, the difference between R1 values of fuel cell with and without the interconnect is calculated. This resistance is the net effect in resistance which is attributed to the interconnect.

Figure 4.4 shows the impedance spectra of fuel cell with NTN material as the interconnect. It appears that the NTN interconnect has a lower resistance than SS441 interconnect which is shown in Figure 4.5. However upon the inspection of the model circuit and calculating the area specific resistances of the interconnects, the electrical resistance of the NTN and SS441 interconnect are similar. Figure 4.6 shows the impedance spectrum of the fuel cell without any interconnect. Indeed, an analysis of the comparison between both the plots will be made further in this section. Comparatively equal interfacial ASR of NTN is mainly attributed to the metal part in ceramic metal composite which provides the electrical conductivity. The resistances of NTN interconnect are shown in Table 4.2. These values in the table are obtained from four different samples that were measured. The impedance spectra of the remaining samples are included in the appendix.

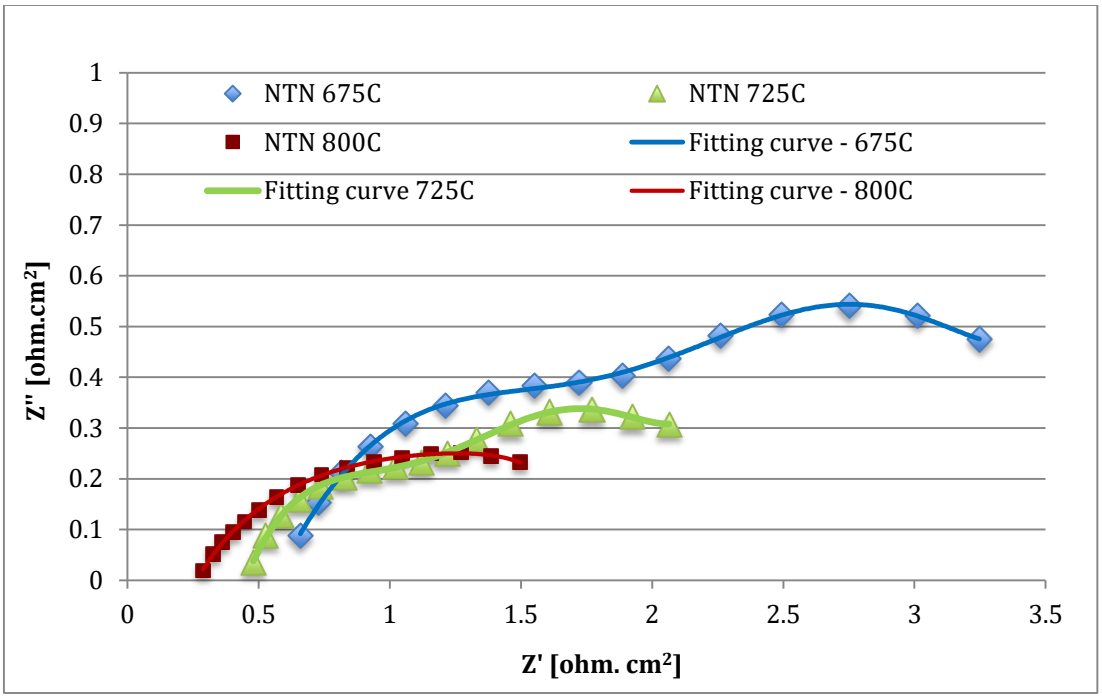

Figure 4.4 Impedance plots of NTN interconnects

Table 4.2 Area specific resistance values for NTN interconnect

Temperature (^{0}C)	R1* resistance (ohm. cm^2)	Error percentage**
675	0.60± 0.1	6.11 ± 3.00
725	0.42±0.07	5.42 ± 3.00
800	0.22± 0.05	2.45 ± 3.41

*R1 resistance corresponds to the resistance of electrolyte, contact resistances and the interconnect

** Error percentage represents the quality of the fitting curve

Figure 4.5 shows the impedance plots of SS441 interconnect at three different temperatures. All the temperatures are selected in the working range of SOFCs. The

measurements were made with an interconnect attached to the cathode of the fuel cell. These values are compared with the impedance values of NTN interconnect. The resistance values for the SS441 interconnect are shown in the Table 4.3.These values are obtained from all the samples that were measured. The impedance spectrum of the remaining samples will be included in the first section of appendix.

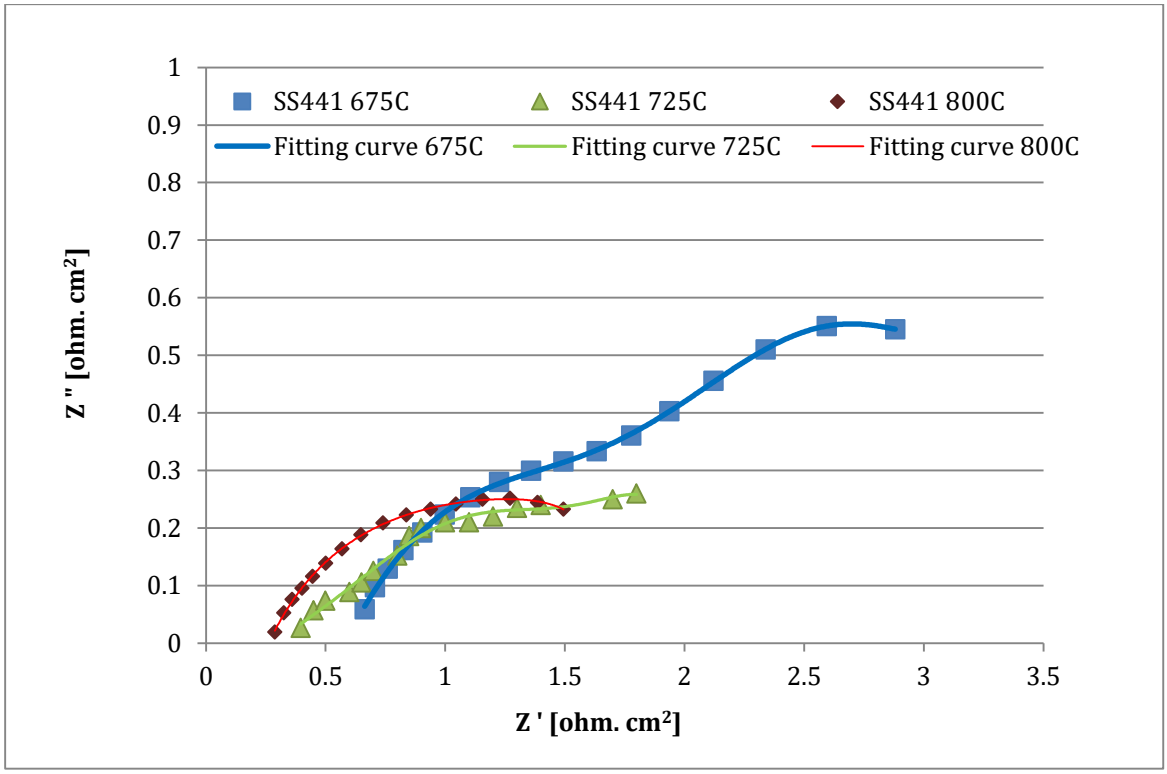

Figure 4.5 Impedance spectrum for SS441 interconnect

Table 4.3 Area specific resistance values for SS441 interconnect

Temperature (^{0}C)	R1* resistance (ohm. cm^2)	Error percentage**
675	0.62 ± 0.09	4.31 ± 3.00
725	0.37 ± 0.1	2.45 ± 3.00
800	0.25 ± 0.07	1.12 ± 3.41

*R1 resistance corresponds to the resistance of electrolyte, contact resistances and the interconnect

** Error percentage represents the quality of the fitting curve

Figure 4.6 shows the impedance plots of fuel cell at three different temperatures. All the temperatures are selected in the working range of SOFCs. The measurements were made without any interconnect attached to the cathode of the fuel cell. The area specific resistance values are shown in Table 4.4. These values are obtained from all the samples that were measured. The impedance spectrum of the remaining samples will be included in the first section of appendix.

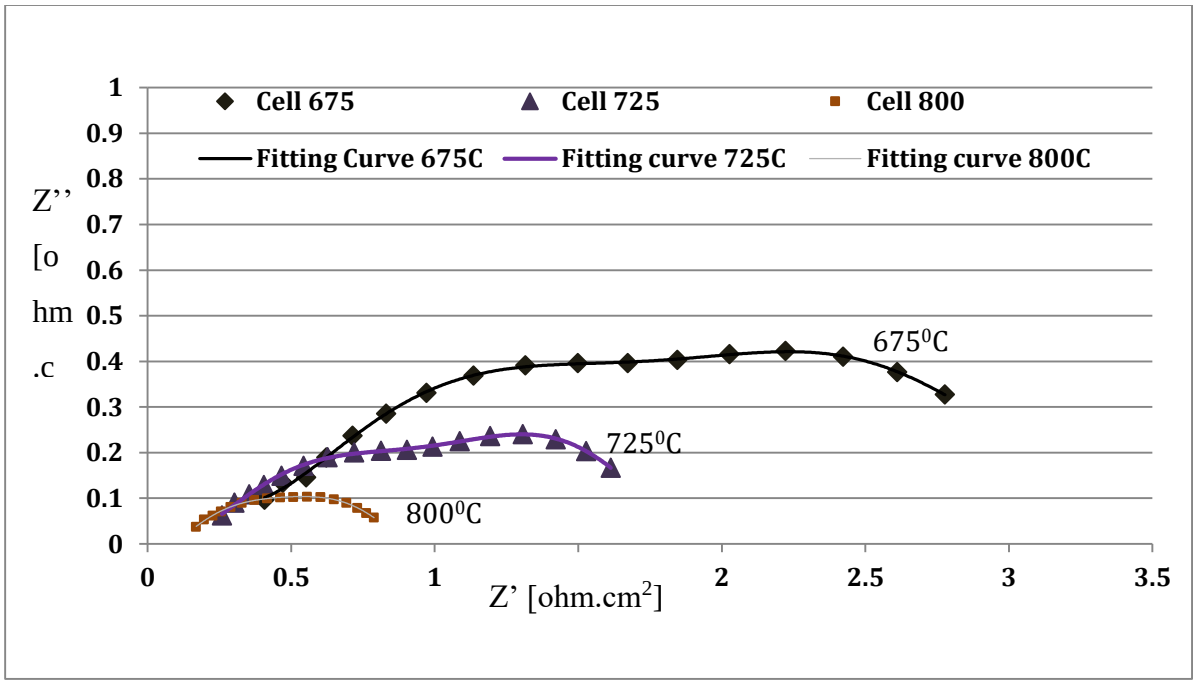

Figure 4.6 Impedance plots for the fuel cell without interconnects

Table 4.4 Area specific resistance values of fuel cells without interconnects

Temperature (^{0}C)	R1* resistance (ohm. cm^2)	Error percentage **
675	0.50 $\pm$ 0.2	4.31 $\pm$ 3.00
725	0.35 $\pm$ 0.08	2.45 $\pm$ 3.00
800	0.15 $\pm$ 0.8	1.12 $\pm$ 3.41

*R1 resistance corresponds to the resistance of electrolyte, contact resistances and the interconnect

** Error percentage represents the quality of the fitting curve

The effect of interconnect resistance on a fuel cell can be studied by analyzing the resistance values of fuel cells with and without the interconnects as a function of temperature. The change in resistance due to the presence of interconnect is shown in the

Table4.5. This table represents the net effective resistance due to different interconnects at different temperatures. At lower temperatures the resistance of both the interconnects is higher. The NTN ceramic metal composite is supposed to have a resistance of 50 milli ohms at 800^0C, which is SS441 interconnect resistance [46]. A comparison between NTN and SS441 interconnects indicates a very similar behavior with respect to their area specific resistances. . Apart from the resistance, the power density characteristics and long-term stability of interconnects are needed for further evaluation of their performance.

Table 4.5 Comparison of NTN and SS441 interconnect resistances

Temperature (^{0}C)	Difference in resistance (NTN and cell) (ohm. cm^2)	Difference in resistance (SS441 and cell) (ohm. cm^2)
675	0.1 ± 0.07	0.12 ± 0.09
725	0.07 ± 0.05	0.02 ± 0.04
800	0.07 ± 0.06	0.09 ± 0.06

4.2. LONG TERM STABILITY

Long-term stability of SOFC stacks is strongly influenced by the characteristics of the interconnect materials and the contact resistance between the cell components. The degradation rate of as stack should be less than 5% for every 1000 hours [2]. Interconnects and the fuel cell considered in this research are planar. Figures 4.7 and 4.8 show a slight increase in the resistance values at 800°C for the NTN and SS441 interconnect after 1500 hours, respectively. The degradation rates for the NTN

metal ceramic composite and SS441 alloy are lower than the required percentages. There was approximately 4% increase in the value of area specific resistance from 100 hours to 1500 hours. This degradation according to the study by Minh et al [2] is acceptable to the current conditions. However, the degradation rates mentioned in reference 2 are for a stack of fuel cells. But in this research however the values taken are for a single interconnect instead of a stack of interconnects and fuel cells. To conclude further on the long term stability for a stack of interconnects, more research has to be done on stacks of interconnects.

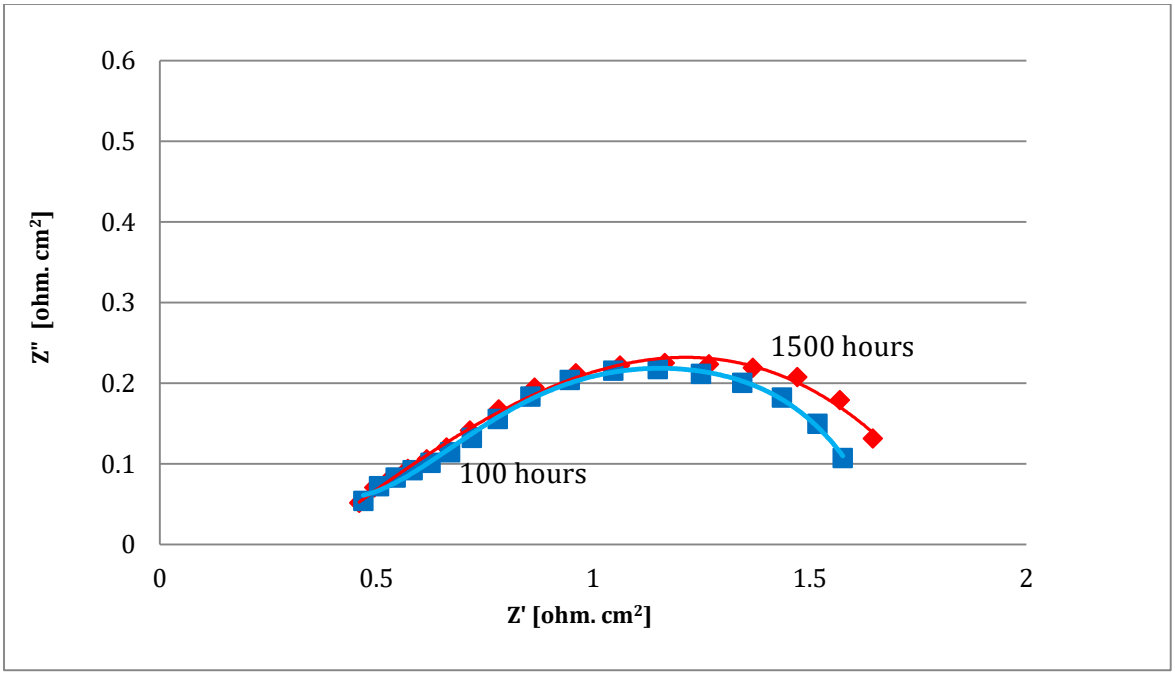

Figure 4.7 Impedance spectra of NTN interconnect after 100 and 1500 hours at 800^0C

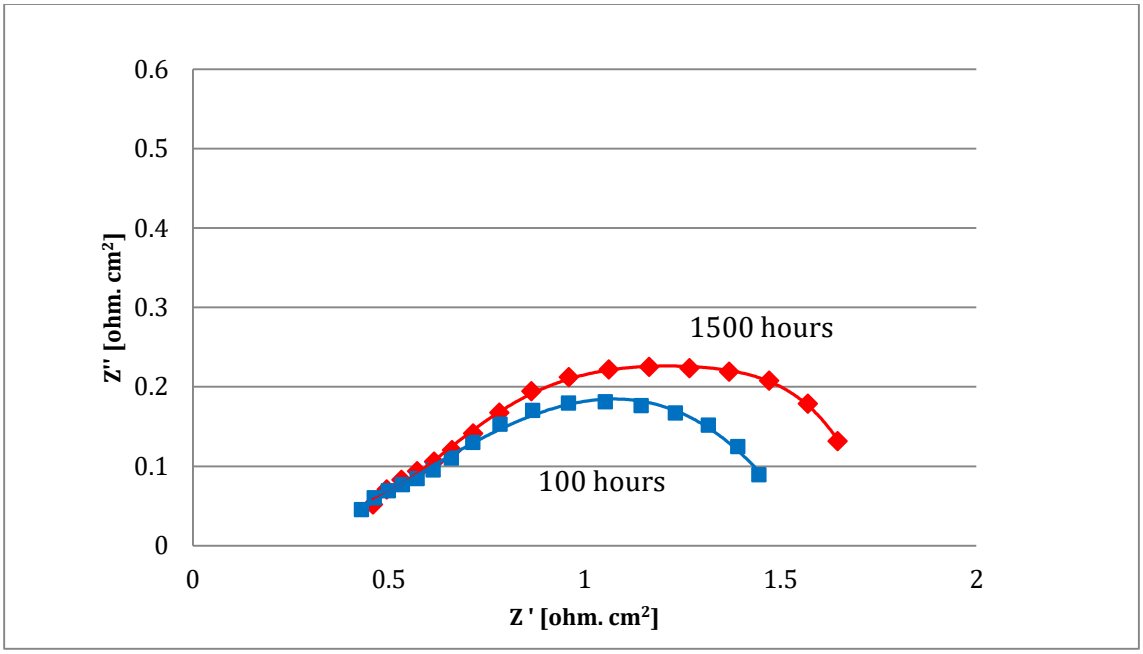

Figure 4.8 Impedance spectra of SS441 interconnect after 100 and 1500 hours

Though a degradation of 0.02 ± 0.01 ohm.cm^2 was seen in SS441 interconnect and NTN, it can be presumed that the difference may be due to poor sealing of the cell or miscellaneous mechanical or electrical contact errors. The degradation rates in Table 4.6 are given in percentages with comparison to that of the value at 100 hours.

Table 4.6 Degradation rates for NTN and SS441 interconnect (relative to the resistance measured after 100 hour)

Time (in hours)	Change in resistance (NTN interconnect + Fuel cell) (ohm.cm^2)	Change in resistance (SS441 interconnect + Fuel cell) (ohm.cm^2)
100	-	-
600	0.009 ± 0.004	0.01 ± 0.005
1500	0.01 ±0.003	0.012 ± 0.007

4.3. POWER DENSITY

Figures 4.9, 4.10 and 4.11 show the power densities and voltage-current characteristics of the cells with NTN composite and SS441 alloy interconnects at different temperatures. Table 4.7 shows the comparison of power density values of NTN and SS441 interconnects. These results clearly indicate that NTN is promising in comparison to SS441 in terms of power density. However, the long-term performance of the cells up to 40,000 hours may show differences by considering the issues with chromium poisoning when SS441 is used as interconnect materials [28]. Such long-term studies need to be conducted to evaluate the performance of both interconnect materials.

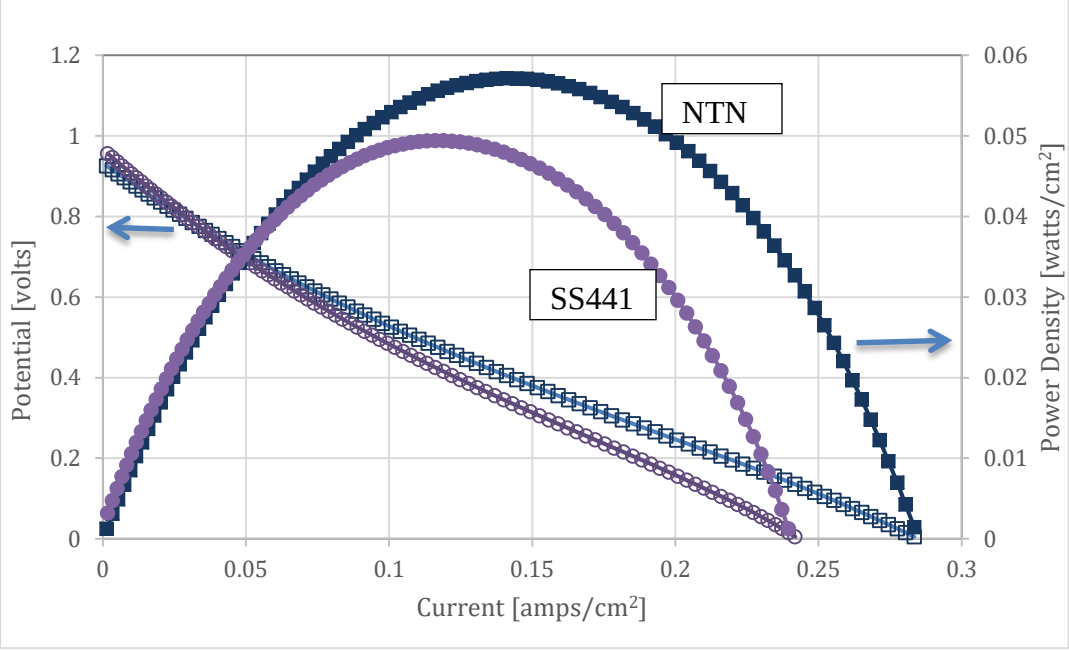

Figure 4.9 Power densities of the cells with NTN and SS441 interconnects at 675^0C after 50 hours of fuel cell test

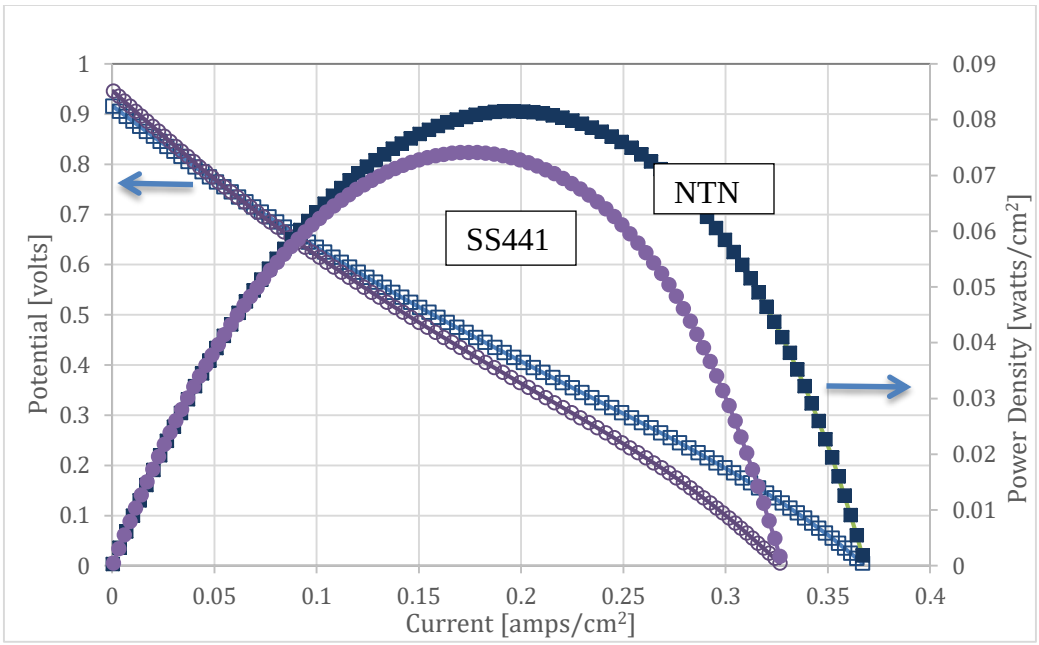

Figure 4.10 Power densities of the cells with NTN and SS441 interconnects at 725^0C

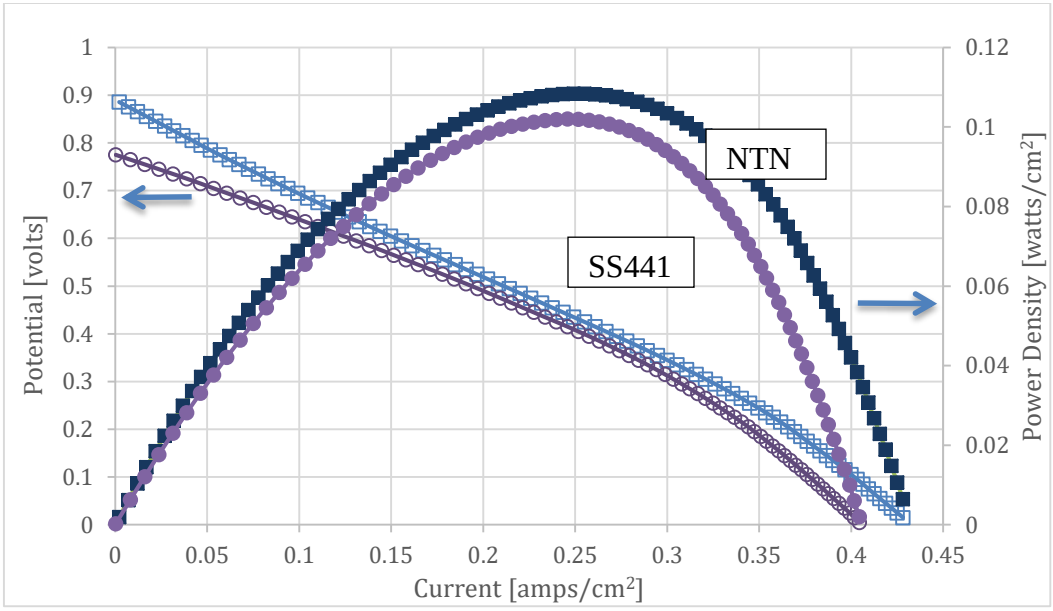

Figure 4.11 Power densities of the cells with NTN and SS441 interconnects at 800^0C

The target power density that is to be achieved is ~0.5watts /cm^2 [2]. The fuel cell supplied has average calculated power density of 0.1 watts/cm^2 at 800^0C. Hence it is not possible to attain anywhere near the targeted power density. But the power densities at different temperatures are given in Table 4.7.

Table 4.7 Power density comparison of SS441 and NTN

Temperature (^{0}C)	Power Density of fuel cell with SS441 (watts/cm^2)	Power Density of fuel cell with NTN (watts/cm^2)
625	0.050 ± 0.03	0.058 ± 0.03
725	0.072 ± 0.03	0.080 ± 0.03
800	0.105 ± 0.04	0.111 ± 0.045

4.4. SEM IMAGES AND EDS ANALYSIS

Figures 4.12 and 4.13 show the microstructure of the fracture surface (cross section) and top surface of the NTN interconnect, respectively. The red circle marked in Figure 4.12 shows the nickel metal in the titanium dioxide ceramic. EDS analysis of the surface and cross-section of the interconnects show that the surface of the interconnect is made of titanium dioxide for chemical stability at higher temperatures. The elemental analysis of the surface of the interconnect (Table 4.8) shows that the surface is made entirely of the ceramic component of the interconnect. The ceramic component provides the mechanical strength and corrosion resistance. All the SEM images are taken as received sample.

Figure 4.14 shows the cross section of solid oxide fuel cells. The figure shows the different components in the fuel cell. The cathode, the electrolyte and the anode are shown in the picture. Figure 4.15 shows the lanthanum strontium manganite, with which the cathode of solid oxide fuel cell used in this research is made and Figure 4.16 shows the lanthanum strontium paste which is used to coat on the interconnect before using the interconnect on the fuel cell. Figure 4.17shows the lanthanum strontium paste which is used to coat on the interconnect after using the interconnect on the fuel cell. It can be clearly seen that the LSM paste looks disintegrated into powder from paste. Figure 4.18 shows the surface of NTN interconnect on which the TiO_2 grains can be seen.

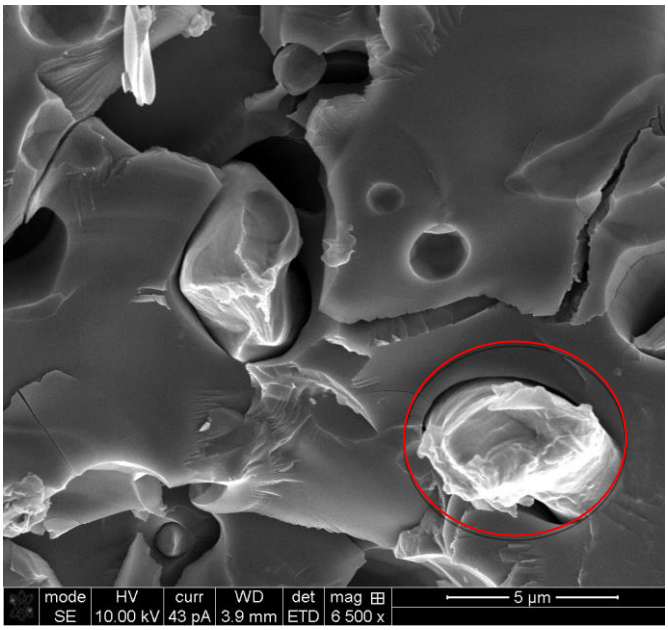

Figure 4.12Fractured surface of NTN interconnect with Ni inclusions in TiO_2 matrix

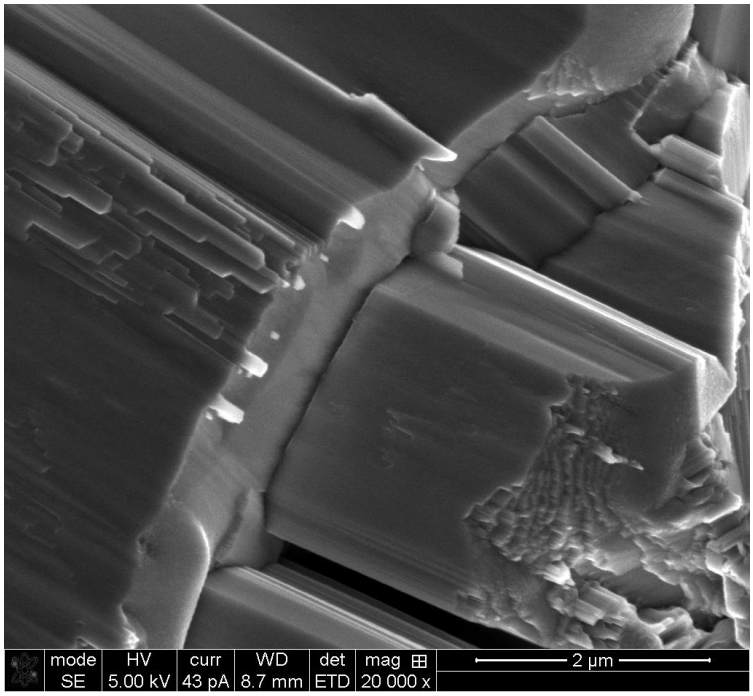

Figure 4.13 Surface of NTN interconnect

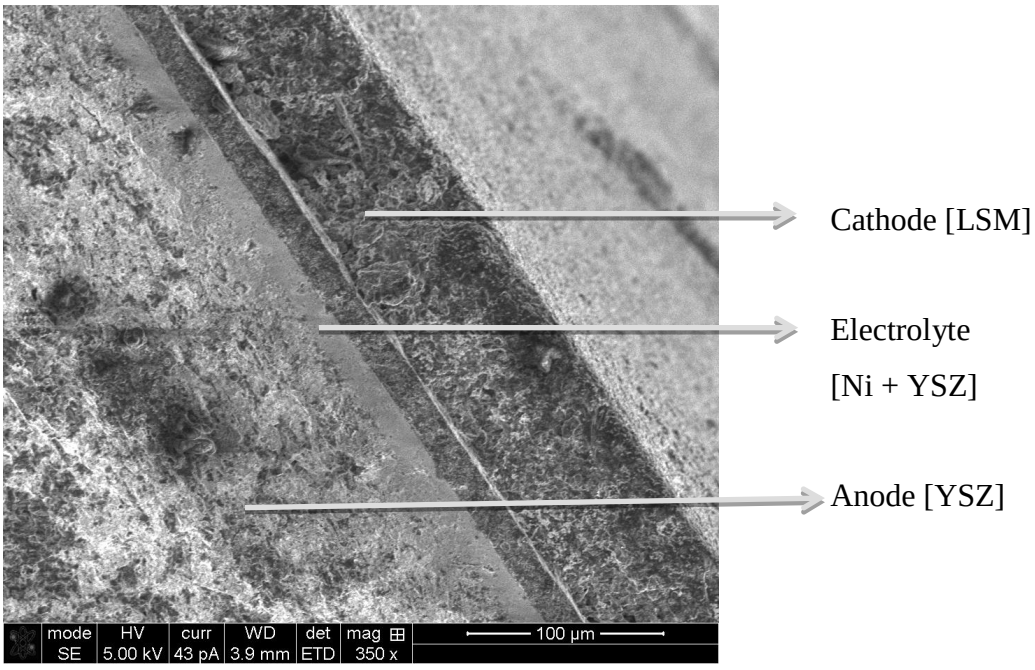

Figure 4.14 Cross section of solid oxide fuel cell

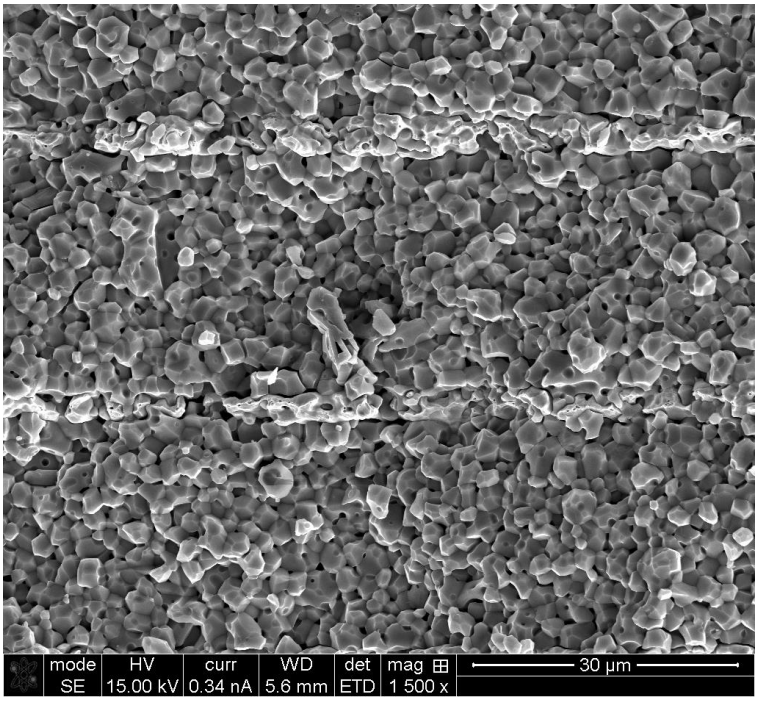

Figure 4.15 Cathode of solid oxide fuel cell (LSM)

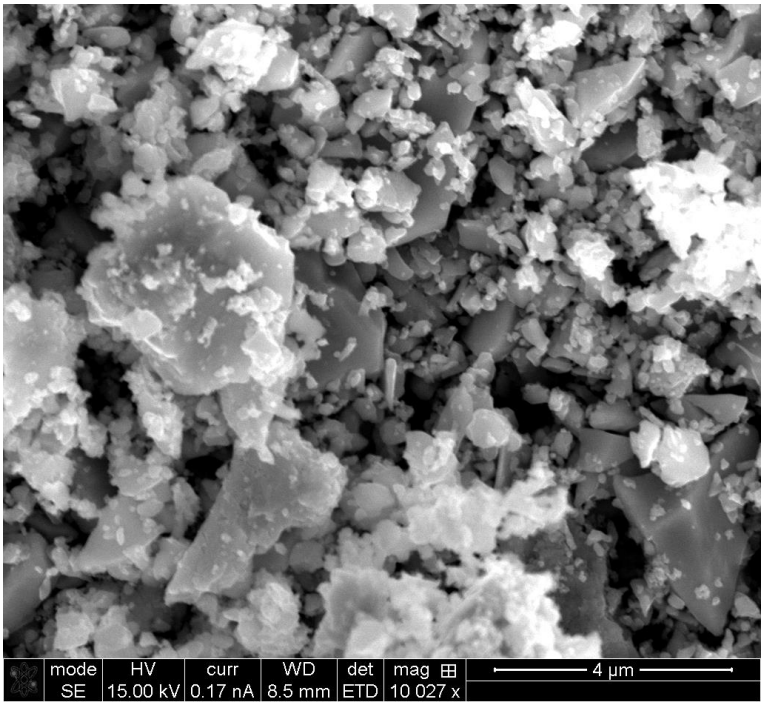

Figure 4.16 LSM contact paste coated on interconnects (before the fuel cell tests)

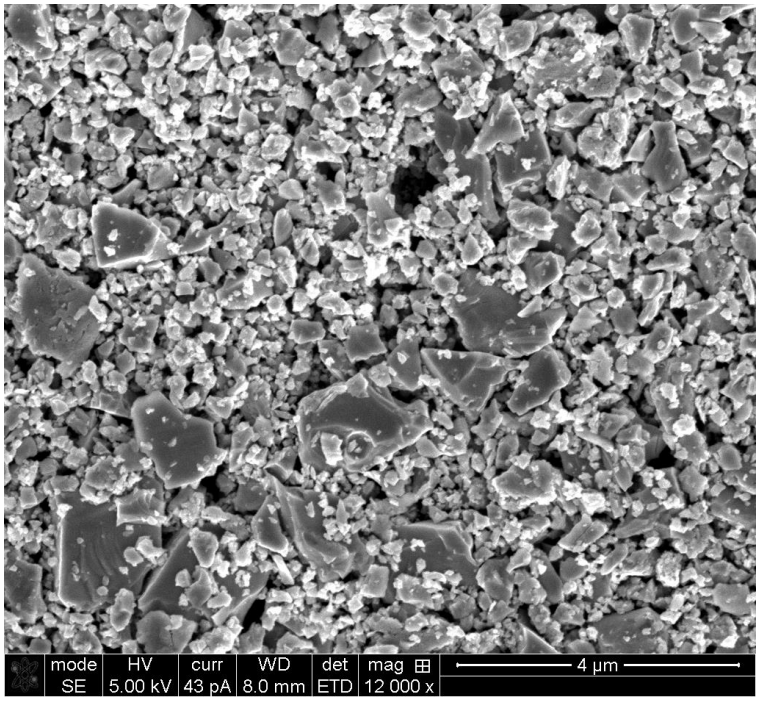

Figure 4.17 LSM contact paste coated on interconnects (after the fuel cell tests)

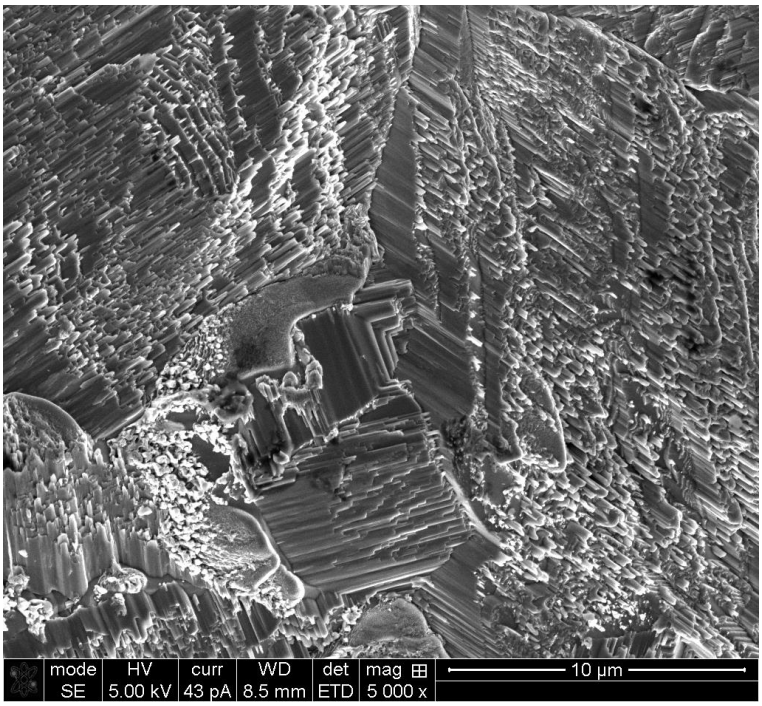

Figure 4.18 NTN interconnect top surface after fuel cell tests for 1500 hours at 800^0C

Table 4.8 Elemental analysis of NTN composite sample surface and cross section

Element	NTN surface		NTN cross section	
	Wt %	At %	Wt %	At %
C*	0.62	1.49	-	-
O	31.66	57.46	25.37	51.78
Ti	67.72	41.05	53.42	36.42
Nb	-	-	0.71	0.30
Ni	-	-	20.51	11.50
Total	100	100	100	100

*Carbon on the interconnect may have shown up from contamination from human interference or from the carbon paste applied to attach the sample to the stub.

4.5. X- RAY DIFFRACTION

Figure 4.19 shows the XRD phase peaks for the NTN interconnect used in this research. The different phase peaks of the sample set shows the different phases of materials present in the interconnect. The phases that are present in ceramic metal composite are the rutile structure of TiO_2 and Nickel.

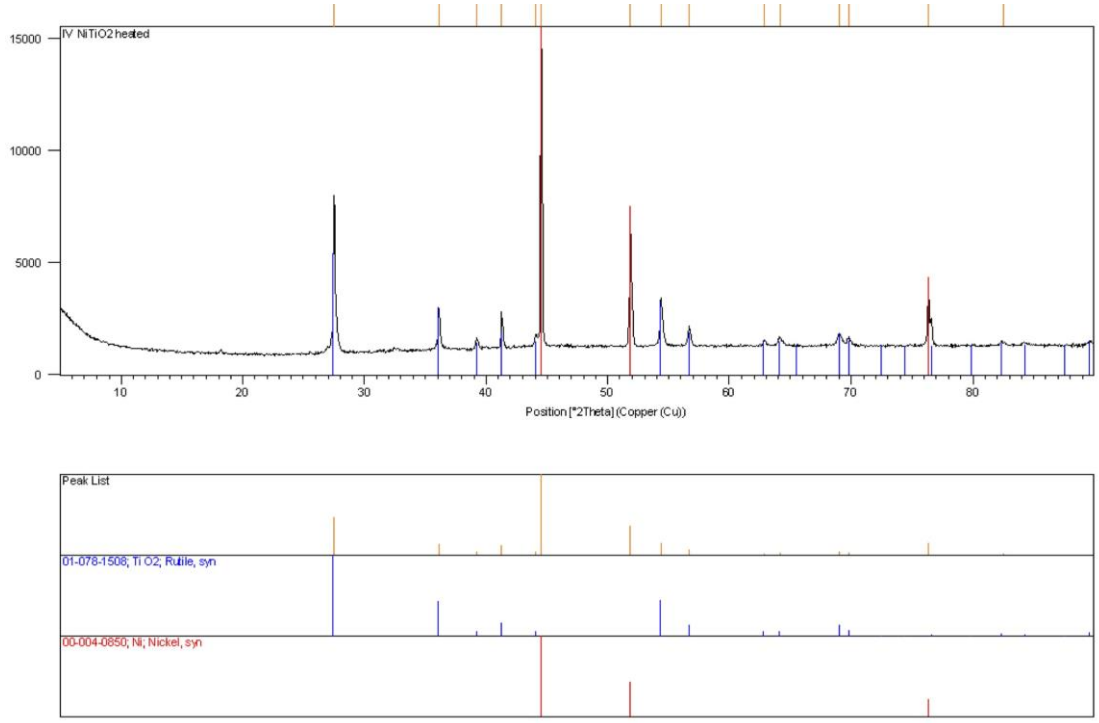

Figure 4.19 XRD pattern for the NTN interconnect with references for rutile (TiO_2) and Ni

5. SUMMARY ANDCONCLUSIONS

The electrical properties of NTN and SS441 materials were compared as an interconnect material for SOFC. The impedance data of NTN and SS441 interconnects obtained from EIS measurements show similar values of electrical performance. Compared to SS441, NTN interconnect is more stable during long term operation of the cells. With the use of LSM paste, the degradation in the performance of both interconnects is less than 5% after 1500 hours. Degradation of performance in area specific resistance using SS441 interconnect is greater than that of NTN and this is attributed to formation of possible volatile compounds of chromium oxides on ferritic steel at elevated temperatures. The change in area specific resistance of NTN ceramic metal composite at 800^0C after 100 hours and 1500 hours is approximately 4% of the value at 100 hours. Though the target power densities (0.5 Watts/cm^2) have not been achieved, the maximum power densities with both interconnects were just higher than 0.11 watts/cm^2. This study shows that NTN composite ceramics are suitable candidates as an interconnect for SOFC stacks with an advantage of absence of chromium poisoning by comparison with ferritic steel based SS441 interconnect alloys.

APPENDIX

The following figure A.1, A.2 and A.3 shows the impedance spectra of the fuel cell with NTN interconnect, without any interconnect and with SS441 interconnect respectively.

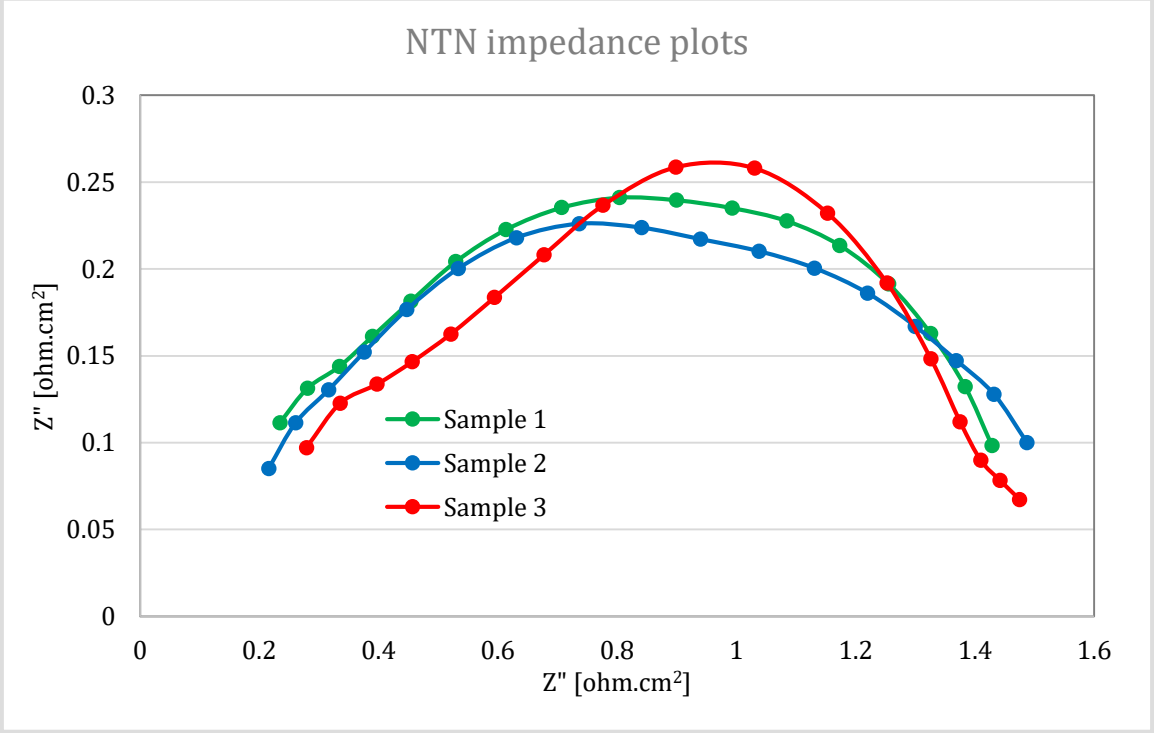

Figure A.1 Impedance spectra of fuel cell with NTN interconnect at 800^0C for different samples after 400 hours

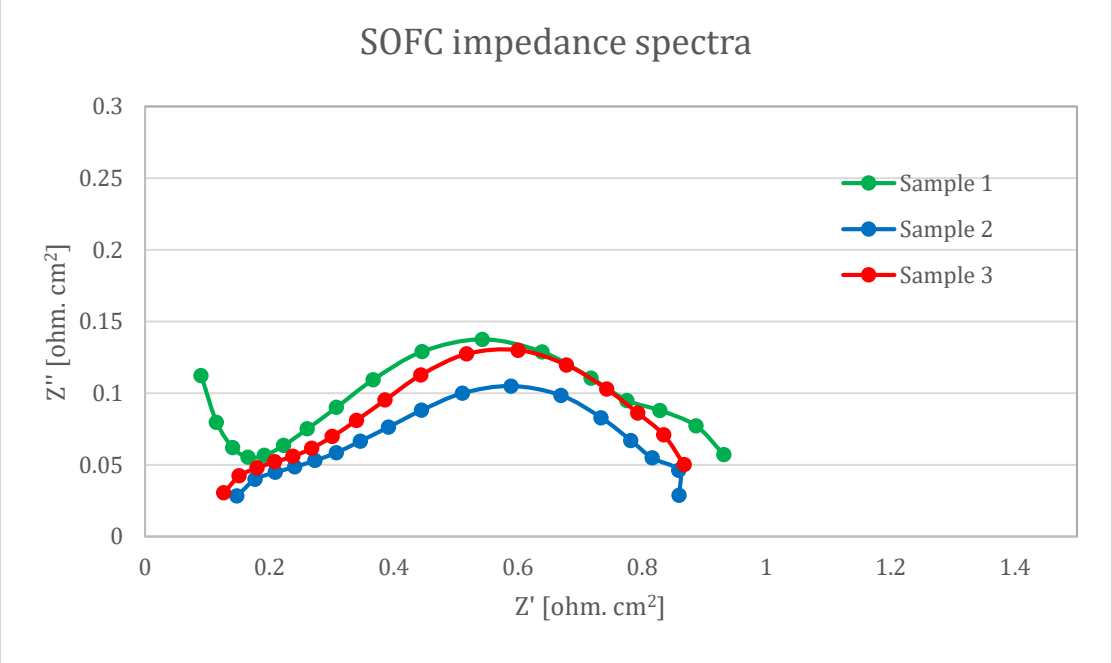

Figure A.2 Impedance spectra of SOFC without interconnect at 800^0C for different samples after 400 hours

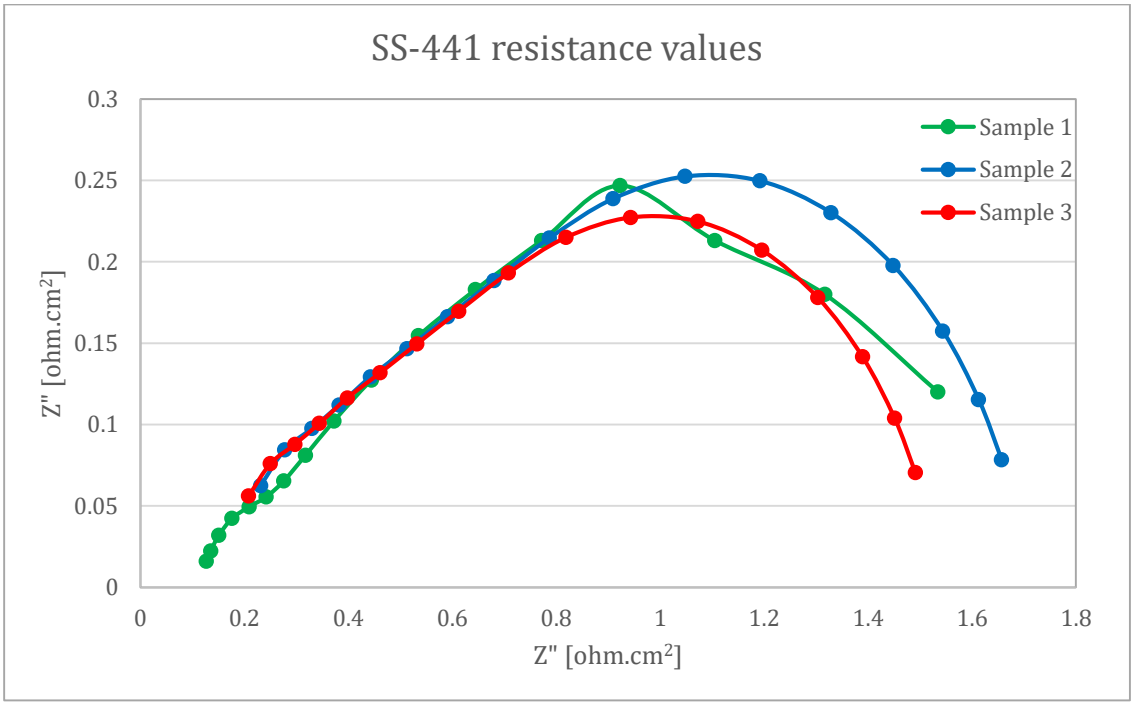

Figure A.3 Impedance spectra of fuel cell with SS441 interconnect at 800^0C for different samples after 400 hours

BIBILOGRAPHY

1. N.Q. Minh, "Solid oxide fuel cell technology, features and applications", *Elsevier, Solid State Ionics*, Vol. 174, Pp. 271-277, (2004).

2. A.B. Stambouli and E. Traversa, "Solid oxide fuel cells (SOFCs): a review of an environmentally clean and efficient source of energy", *Renewable and Sustainable Energy Reviews*, Vol. 6, Pp. 433–455, (2002).

3. E. Riensche, E. Achenbach, D. Froning, M.R. Haines, W.K. Heidug, A. Lokurlu et al, "Clean Combined Cycle SOFC Power Plant - Cell Modelling and Process Analysis", *Journal of Power Sources*, Vol.86 [1–2], Pp. 404-410, (2000).

4. M. Santin, A. Traverso, L. Magistri and A.F. Massardo, "Analysis of SOFC–GT Hybrid Systems Fed by Liquid Fuels", *Energy Journal*, Vol.35, Pp. 1077-1083, (2010).

5. E.D. Wachsman and K.T. Lee, "Lowering the Temperature of Solid Oxide Fuel Cells", *Science Journal*, Vol. 334, Pp. 935-939, (2011).

6. R.M. Ormerod, "Solid oxide fuel cells", *Chemical Society Reviews, Science Journal* Vol.32, Pp. 17-28, (2011).

7. J.P. Trembly, A.I. Marquez, T.R. Ohm and D.J. Bayless, "Effects of coal syngas and H_2S on the performance of solid oxide fuel cells: Single-cell tests", *Journal of Power Sources*, Vol. 158,Pp. 263-273, (2006).

8. Wenying and Yixiang Shi, "Carbon deposition on patterned nickel/yttria stabilized zirconia electrodes for solid oxide fuel cell/solid oxide electrolysis cell modes", *Journal of Power Sources*, Vol.276, Pp. 26-31, 2015.

9. O. Kubaschewski and C. B. Alcock, *Metallurgical Thermochemistry*, 5th edn, Oxford Pubs: UK, 1979.

10. W.Z. Zhu and S.C. Deevi, "Development of interconnect materials for solid oxide fuel cells", *Material Science Engineering Journal*, Vol. A345, Pp. 227-243, (2002).

11. J. W. Fergus, R. Hui and X. Li, "Solid oxide fuel cells – materials properties and performance", CRC press: USA, (2009).

12. J.G. Grolig, J. Froitzheim and J.E. Svensson, "Coated stainless steel 441 as interconnect material for solid oxide fuel cells: Oxidation performance and chromium evaporation", *Journal of Power Sources*, Vol. 248, Pp. 1007–1013, (2014).

13. J.W. Fergus, “Lanthanum Chromite based materials for solid oxide fuel cell interconnects”, *Solid State Ionics,* Vol. 171, Pp. 1-15, (2004).

14. Z. Yang, K.S. Weil, D. Paxton and J.W. Stevenson, “Selection and evaluation of heat resistant alloys for solid oxide fuel cell interconnect applications”, *Journal of Electrochemical Society*, Vol. 150, Pp. A1188-A1201, (2003).

15. T.C Wei and Philips, “Thermal and Catalytic Etching: Mechanisms of Metal Catalyst Reconstruction”, *Journal of Advancement in Catalysis*, Vol. 41, Pp. 359-421, (1996).

16. X. Bao, G. Lehmpfuhl, R. Scholgl and G. Erts, “Variation of the morphology of silver surfaces by thermal and catalytic etching”, *Journal of Chemical Society Faraday Trans*, Vol. 88, Pp. 865-872, (1992).

17. W. Qu, L. Jian, J.M. Hill and D.G. Ivey, “Electrical and microstructural characterization of spinel phases as potential coatings for SOFC metallic interconnects”, *Journal of Power Sources*, Vol. 153, Pp. 114–124, (2006).

18. R. Eriksen, S. Gopalan, S. Sampath and Y. Chen (2014), “LSM protective coatings on stainless steel as interconnects for solid oxide fuel cells”, *MRS Proceedings,* Vol. 1644, (2014).

19. J.W. Fergus, “Metallic interconnects for solid oxide fuel cells”, *Journal of Material Science*, Vol. A397, Pp. 271-283, (2005).

20. T. Nakamura, G. Petzow and L.J. Hauckler, “Stability of perovskite based $LaBO_3$ (B=V, Cr, Mn, Fe, Co, Ni) in reducing atmosphere”, I. *Experimental results, Mater Research Bulletin,* Vol. 14, Pp. 649-659, (1979).

21. R. Weiss, D. Peck, M. Miller and K. Hilpert, “Volatility of chromium from interconnect material in high temperature electrochemistry: ceramics and metals”, *Proceedings of the 17th Riso international symposium on materials science. Roskilde, Denmark: Riso National Lab*., Pp. 479–484, (1996).

22. E. Konycheva, H. Penkalla, E. Wessel, U. Seeling, L. Singheiser and K. Hilpert “Comparison of chromium poisoning by the ODS alloy Cr5FeY2O3 and the high chromium ferritic steel Crofer 22 APU”, *Proceedings of Electrochemical Society*, Pp. 1874–1884, (2005).

23. C. Gindorf, L. Singheiser and K. Hilpert, “Chromium vaporization from Fe, Cr base alloys used as interconnect in fuel cells”, *Steel Research Journal,* Vol. 72, Pp. 528–533, (2001).

24. C. Gindorf, L. Singheiser, K. Hilpert, M. Schroeder, M. Martin, H. Greiner et al. "Chromium vaporization from metallic interconnect and retention by perovskite layers", *Proceedings of Electrochemical Society*, Vol. 19(SOFC VI), (1999).

25. S.P.S. Badwal, R. Deller, K. Foger, Y. Ramprakash and J.P. Zhang, "Interaction between chromia forming alloy interconnects and air electrode of solid oxide fuel cells", *Solid State Ionics*, Vol. 99, Pp. 297-310, (1997).

26. E. Konysheva, H. Penkalla, E. Wessel, J. Mertens, U. Seeling, L. Singheiser, et al. "Chromium poisoning of perovskite cathodes by the ODS alloy Cr5Fe1Y2O3 and the high chromium ferritic steel Crofer22APU", *Journal Electrochemical Society*, Vol. 153, Pp. A765–A773, (2006).

27. Y. Matsuzaki, M. Hishinuma and I. Yasuda, "Complex impedance analysis of SOFC cathode and its application to investigate the Cr-poisoning", *Electrochemical Society Proceedings*, Volume 19 (SOFC VI), (1999).

28. K. Fujita, K. Ogaswara, Y. Matsuzaki and T. Sakura, "Prevention of SOFC cathode degradation in contact with Cr-containing alloy", *Journal Power Sources*, Vol. 131, Pp. 261–269, (2004).

29. K. Fujita, T. Hashimoto, K. Ogasawara, H. Kameda, Y. Matsuzaki and T. Sakurai, "Relationship between electrochemical properties of SOFC cathode and composition of oxide layer formed on metallic interconnects", *Journal Power Sources*, Vol. 131, Pp. 270-277, (2004).

30. M. Dokiya, and S. C. Singhal, "Solid Oxide Fuel Cells", *Proceedings of Electrochemical Society*, Vol.19 (SOFC VI), Pp. 981–990, (1999).

32. S. Taniguchi, M. Kadowaki, H. Kawamura, T. Yasuo, Y. Akiyama, Y. Miyake, et al., "Degradation phenomena in the cathode of a solid oxide fuel cell with an alloy separator", *Journal of Power Sources*, Vol. 55, Pp. 73–79, (1995).

33. N. Shaigan and W. Qu, "A review of recent progress in coatings, surface modifications and alloy developments for solid oxide fuel cell ferritic stainless steel interconnects", *Journal of Power Sources*, Vol. 175, Pp. 1529–1542, (2010).

34. K. Huang, P.Y. Hou and J.B. Goodenough, "Reduced Area Specific Resistance for Iron- based Metallic Interconnects by Surface Oxide Coatings", *Materials Research Bulletin*, Vol. 36, Pp. 85-91, (2001).

35. W. Qu, H. Li and D.G. Ivey, "Synthesis of La0.7Sr0.3MnO3 thin films supported on Fe–Cr alloy by sol–gel/dip-coating process: Evaluation of deposition parameters", *Journal of Power Sources*, Vol. 138, Pp. 162–173, (2004).

36. W. Qu, L. Jian, D.G. Ivey, J.M. Hill, "Yttrium, cobalt and yttrium/cobalt oxide coatings on ferritic stainless steels for SOFC interconnects", *Journal of Power Sources*, Vol. 157, Pp. 335–350, (2006).

37. N. Oishi, T. Namikawa and Y. Yamazaki, "Oxidation behavior of an La-coated chromia-forming alloy and the electrical property of oxide scales", *Surface & Coatings Technology*, Vol. 132, Pp. 58-64, (2000).

38. D.E. Alman and P.D. Jablonski, "Effect of minor elements and a Ce surface treatment on the oxidation behavior of an Fe–22Cr–0.5Mn (Crofer 22 APU) ferritic stainless steel", *International Journal of Hydrogen Energy*, Vol. 32, Pp. 3743–3753, (2007).

39. J.J. Choi, J.H. Lee, D.S. Park, B.D. Hahn, W.H. Yoon and H.T. Lin, "Oxidation Resistance Coating of LSM and LSCF on SOFC Metallic Interconnects by the Aerosol Deposition Proces", *Journal of the American Ceramic Society*, Vol. 90, Pp. 1926–1929, (2007).

40. J.J. Choi, D.S. Park, B.D. Hahn, J. Ryu and W.H. Yoon, "Oxidation Behavior of Ferritic Steel Alloy Coated with Highly Dense Conducting Ceramics by Aerosol Deposition", *Journal of the American Ceramic Society*, Vol. 91, Pp. 2601–2606, (2008).

41. B. Hua, J.F. Zhang, F.S. Lu, Y.H. Kong, J. Pu, J. Li, "Electrophoretic deposition of ZnCo2O4 spinel and its electrocatalytic properties for oxygen evolution reaction", *Acta Metallurgica Sinica*, Vol. 45, Pp. 605–609, (2009).

42. A. Petric and P. Huang, "Evaluation of La–Sr–Co–Fe–O perovskites for solid oxide fuel cells and gas separation membranes", *Solid State Ionics*, Vol. 135, Pp. 719-725, (2000).

43. C.J. Fu, K.N. Sun, N.Q. Zhang and D.R. Zhou, "Effects of Protective Coating Prepared by Atmospheric Plasma Spraying on Planar SOFC Interconnect", *Rare Metal Materials and Engineering*, Vol. 35, Pp. 1117–1120, (2006).

44. C. Johnson, R. Gemmen and N. Orlovskaya, "Nano-structured self-assembled LaCrO3 thin film deposited by RF-magnetron sputtering on a stainless steel interconnect material", *Composites Part B-Engineering*, Vol.35, Pp. 167–172, (2004).

45. Y.J. Yang, T.L. Wen, H.Y. Tu, D.Q. Wang and J.H. Yang, "Characteristics of lanthanum strontium chromite prepared by glycine nitrate process", *Solid State Ionics*, Vol.135 , Pp. 475–479, (2000).

46. Z.G. Yang, G.G. Xia, G.D. Maupin and J.W. Stevenson, "Evaluation of Perovskite Overlay Coatings on Ferritic Stainless Steels for SOFC Interconnect Applications", *Journal of the Electrochemical Society*, Vol. 153, Pp. A1852–A1858, (2006).

47. N. Orlovskaya, A. Coratolo, C. Johnson and R. Gemmen, “Structural evolution of La–Cr–O thin films: Part I. Microstructure and phase development,’’ *Thin solid films*, Vol. 515, Pp. 1741-1747, (2006).

48. I. Belogolovsky, X.D. Zhou, H. Kurokawa, P.Y. Hou, S. Visco and H.U. Anderson, “Effects of Surface Deposited Nanocrystalline Chromite Thin Films on the Performance of a Ferritic Interconnect”, *Journal of the Electrochemical Society*, Vol. 154, Pp. B976–B980, (2007).

49. M.R. Bateni, P. Wei, X.H. Deng and A. Petric, “Spinel coatings for UNS 430 stainless steel interconnects”, *Surface & Coatings Technology*, Vol. 201, Pp. 4677–4684, (2007).

50. J.J. Choi, J. Ryu, B.D. Hahn, W.H. Yoon, B.K. Lee and D.S. Park, “Dense spinel MnCo2O4 film coating by aerosol deposition on ferritic steel alloy for protection of chromic evaporation and low-conductivity scale formation”, *Journal of Materials Science*, Vol. 44, Pp. 843–848, (2009).

51. B. Hua, J.A. Pu, W. Gong, J.F. Zhang, F.S. Lu and L. Jian, “Cyclic oxidation of Mn–Co spinel coated SUS 430 alloy in the cathodic atmosphere of solid oxide fuel cells”, *Journal of Power Sources*, Vol. 185, Pp. 419–422, (2008).

52. C.C. Mardare, H. Asteman, M. Spiegel, A. Savan and A. Ludwig, “Investigation of thermally oxidised Mn–Co thin films for application in SOFC metallic interconnects”, *Applied Surface Science*, Vol. 255, Pp. 1850–1859, (2008).

53. X. Montero, N. Jordan, J. Piron-Abellan, F. Tietz, D. Stover, M. Cassir and I. Villarreal, “Spinel and Perovskite Protection Layers Between Crofer22APU and La0.8Sr0.2FeO3 Cathode Materials for SOFC Interconnects”, *Journal of the Electrochemical Society*, Vol. 156, Pp. B188–B196, (2009).

55. P. Wei, X. Deng, M.R. Bateni and A. Petric, “Oxidation and Electrical Conductivity Behavior of Spinel Coatings for Metallic Interconnects of Solid Oxide Fuel Cells”, *Corrosion Journal*, Vol. 63, Pp. 529–536, (2007).

56. W.F. Wei, W.X. Chen and D.G. Ivey, “Oxidation resistance and electrical properties of anodically electrodeposited Mn–Co oxide coatings for solid oxide fuel cell interconnect applications”, *Journal of Power Sources*, Vol. 186, Pp. 428–434, (2009).

57. S. W. Paulik, S. Baskaran and T. R. Armstrong, “Mechanical properties of calcium and strontium based lanthanum chromite”, *Journal of material sciences*, Vol: 33, Pp. 2397-2404, (1997).

58. I. Yasua and M. Hishinuma, “Lattice expansion of acceptor-doped lanthanum chromites under high temperature reducing atmospheres”, *Journal of Electrochemistry* (Tokyo), Vol : 68, Pp. 526-530, (2000).

59. M. Mori and Y. Hiei, “Thermal expansion behavior of titanium doped La(Sr)CrO3 solid oxide fuel cell interconnects”, *Journal of American Ceramic Society*, Vol :84, Pp. 2573-2578, (2001).

60. D. S. Smith, M. Sayer and P. Odier, “The formation and characterization of ceramic-ceramic interface between stabilized zirconia and lanthanum chromite”, *Journal of Physique Colloque*, Vol: C1, Pp. 150-157, (1986).

61. J. D. Carter, C. C. Appel and M. Mongensen, “Reactions at the calcium doped lanthanum chromite-yttria stabilized zirconia interface”, *Journal of Solid State Chemistry*, Vol: 122, Pp. 407-415, (1996).

62. T. Yamamoto, H. Itoh, M. Mori, N. Mori, T. Watanab et al, “Property of (La,Ca)CrO3 for interconnect in solid oxide fuel cell”, *Journal of Ceramic Society*, Vol : 109, Pp. 527-534, (2001).

63. C. E. Hatchwell, N. M. Sammes and I. W. M. Brown, “Chemical compatibility of Chromium based interconnect related materials with doped cerium oxide electrolyte”, *Journal of European Ceramic Society*, Vol: 19, Pp. 1697-1703, (1999).

VITA

Abhijith Budur was born on January 22, 1993 in Kurnool, India. He received his Bachelor of Science Degree in Metallurgical Engineering from Jawaharlal Nehru Technological University in May 2013 after several co-ops and internships at international industrial companies and research institutes. Right after the graduation he worked for over six months at mineral companies in India. After that he started pursuing his Masters in Spring 2014 under the supervision of Dr. Fatih Dogan in Missouri University of Science and Technology (formerly University of Missouri – Rolla) in Rolla, Missouri, U.S.A. His master's work was focused on the analysis of the Nickel-Titanium Dioxide-Niobium Pentoxide interconnect for solid oxide fuel cell. In August 2015 he received his MS in Material Sciences and Engineering form Missouri University of Science and Technology.